Plasmonics
https://doi.org/10.1007/s11468-024-02620-x

REVIEW

Developments in Localized Surface Plasmon Resonance

M. P. Mcoyi[1] · K. T. Mpofu[1] · M. Sekhwama[1] · P. Mthunzi-Kufa[1,2,3]

Received: 30 August 2024 / Accepted: 17 October 2024

Abstract
Localized surface plasmon resonance (LSPR) is a nanoscale phenomenon associated with noble metal nanostructures that has long been studied and has gained considerable interest in recent years. These resonances produce sharp spectral absorption and scattering peaks, along with strong electromagnetic near-field enhancements. Over the past decade, advancements in the fabrication of noble metal nanostructures have propelled significant developments in various scientific and technological aspects of LSPR. One notable application is the detection of molecular interactions near the nanoparticle surface, observable through shifts in the LSPR spectral peak. This document provides an overview of this sensing strategy. Given the broad and expanding scope of this topic, it is impossible to cover every aspect comprehensively in this review. However, we aim to outline major research efforts within the field and review a diverse array of relevant literature. We will provide a detailed summary of the physical principles underlying LSPR sensing and address some existing inconsistencies in the nomenclature used. Our discussion will primarily focus on LSPR sensors that employ metal nanoparticles, rather than on those utilizing extended, fabricated structures. We will concentrate on sensors where LSPR acts as the primary mode of signal transduction, excluding hybrid strategies like those combining LSPR with fluorescence. Additionally, our examination of biological LSPR sensors will largely pertain to label-free detection methods, rather than those that use metal nanoparticles as labels or as means to enhance the efficacy of a label. In the subsequent section of this review, we delve into the analytical theory underpinning LSPR, exploring its physical origins and its dependency on the material properties of noble metals and the surrounding refractive index. We will discuss the behavior of both spherical and spheroidal particles and elaborate on how the LSPR response varies with particle aspect ratio. Further, we detail the fundamentals of nanoparticle-based LSPR sensing. This includes an exploration of single-particle and ensemble measurements and a comparative analysis of scattering, absorption, and extinction phenomena. The discussion will extend to how these principles are applied in practical sensing scenarios, highlighting the key experimental approaches and measurement techniques.

Keywords Localized surface plasmon resonance (LSPR) · Nanoparticles · Plasmonic sensing · Biosensing applications · Surface plasmon resonance (SPR)

Abbreviations

AChE	Acetylcholinesterase
ADDL	Amyloid-beta-derived diffusible ligand
AFM	Atomic force microscopy
Ag	Silver
AIDS	Acquired immunodeficiency syndrome
Au	Gold
Cd	Cadmium
ConA	Concanavalin A
Cu	Copper
DDA	Discrete dipole approximation
DiNM	Digital nanoplasmon-metry
DNA	Deoxyribonucleic acid
DNP	Dinitrophenyl
EB	Electron beam
EDCs	Endocrine disrupting chemicals
ELISA	Enzyme-linked immunosorbent assay
EM	Electromagnetic
EOT	Extraordinary optical transmission

✉ K. T. Mpofu
kmpofu@csir.co.za

[1] Council for Scientific and Industrial Research (CSIR), National Laser Centre, Pretoria, South Africa

[2] Molecular and Cell Biology Department, University of Cape Town, Cape Town 7701, South Africa

[3] School of Interdisciplinary Research and Graduate Studies (UNESCO), College of Graduate Studies, University of South Africa, Preller Street, Muckleneuk Ridge, Pretoria, South Africa

Published online: 04 November 2024

FDTD	Finite difference time domain
FEM	Finite element method
FOM	Figure of merit
GAs	Genetic algorithms
GBP	Gold-binding polypeptide
Hg	Mercury
HIV	Human immunodeficiency virus
ICP-MS	Inductively coupled-plasma mass spectrometry
In	Indium
LCTF	Liquid crystal tunable filter
LED	Light-emitting diode
LPFG	Long-period fiber grating
LSP	Localized surface plasmon
LSPR	Localized surface plasmon resonance
MDL	Molecular detection limit
ML	Machine learning
MNP	Metal nanoparticle
NIL	Nanoimprint lithography
NIR	Near-infrared
nm	Nanometers
NP	Nanoparticle
NSL	Nanosphere lithography
NSOM	Near-field scanning optical microscopy
Pb	Lead
PBs	Polychlorinated biphenyls
PCA	Principal component analysis
Pd	Palladium
PHI	Photothermal heterodyne imaging
PMMA	Poly(methyl methacrylate)
PS	Polystyrene
PSS	Polystyrene sulfonic acid
Pt	Platinum
QE	Quantum emitter
RI	Refractive index
RIU	Refractive index unit
RNA	Ribonucleic acid
SAMs	Self-assembled monolayers
SERS	Surface-enhanced Raman spectroscopy
Sn	Tin
SPPs	Surface plasmon polaritons
SPR	Surface plasmon resonance
SVM	Support vector machines
TEM	Transmission electron microscopy
Ti	Titanium
VIS	Visible
VOCs	Volatile organic compounds

Introduction

Since the fourth century A.D., noble metal nanoparticles, often composed of silver, copper, aluminum, and gold, have been useful in various ways [1]. Unlike other materials, these noble metal nanoparticles can absorb and scatter light in specific regions in the visible spectrum [2]. The ability to generate coherent electric field enhancements and radiative decay through the oscillation of electrons on a nanoparticle's surface is a promising tool for analyzing and transporting molecules. Noble metal nanoparticles have been widely used in various fields, such as biosensors, catalytic materials, and electro-optic and semiconducting devices [3]. The localized surface plasmon resonance (LSPR) biosensor describes the famous application of these nanoparticles in biosensors. In LSPR-based sensing, the interaction of light with noble metal nanoparticles leads to a collective oscillation of electrons in the conduction band, known as LSPR [4]. The oscillations of electrons in a solid are known as plasmons. When the plasma excitation threshold is met, the volume or bulk plasmon polariton propagates in different dimensions. The first is the incoming energy quanta, while the second is the plasma frequency of the medium [5]. These noble metal nanoparticles create non-propagating surface plasmons, and thus, the surface plasmons are localized. The non-propagating surface plasmons generate a short field decay duration of around 10 to 30 nm [6]. The short field decay length makes the LSPR sensor ideal for detecting small changes in the surface's refractive index. The molecules that bind to the surface affect the plasmonic resonance, and this change in the surface plasmon of the nanoparticle's surface allows for the detection of an altered plasmonic signal [6]. Studies are also being conducted on the analytical applications field of metallic nanoparticle interaction with rare-earth ions [7].

When light passes through LSPs at a certain wavelength, resonance can occur, as indicated in Fig. 1. This phenomenon results in the appearance of surface plasmon absorption

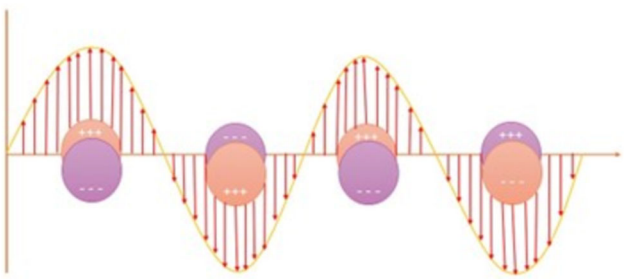

Fig. 1 Diagram illustration of localized surface plasmon resonance on the sensor surface

bands, which are characterized by their intensity and position. These surface plasmons are highly sensitive to environmental changes [1]. This method can detect an increase in the thickness of the biomolecular layer on the surface of a sensitive component due to a reaction between a solution component and the receptor layer, as a change in the surface plasmon. This approach can further be applied to observe the reactions between different ligands, such as antigen and antibody reactions. Mostly, materials with a small positive dielectric constant can support surface plasmons [4]. Most commonly, silver and gold nanoparticles are adopted to support surface plasmons. However, other metals such as aluminum and copper can also exhibit this phenomenon. When an electromagnetic field interacts with the electrons on the surface of a nanoparticle, a resonance condition is formed. The increase in an electromagnetic field, absorption field, and nanoparticle surface scattering due to resonant oscillations is used for sensing applications [1]. The gains in these parameters have been particularly beneficial in the analysis of biological analytes and further for surface-enhanced Raman spectroscopy (SERS). The changes in the LSPR peaks caused by the changes in the materials' dielectric properties can be correlated with the changes in the refractive index and extinction coefficient of the surrounding medium. This characteristic alone can be used as a plasmonic sensor [8].

The phenomenon of LSPR has been studied and reported for a long time. It is associated with noble metal nanostructures and generates strong near-field electromagnetic enhancements. The development of LSPR technology and the fabrication of these noble metal nanostructures have led to various advancements in science. One of the most common applications of LSPR is the detection of molecules near the surface of a nanoparticle. It can be done by using a variety of materials, such as metal nanoparticles. There are also hybrid strategies that combine the features of LSPR and fluorescence. Instead of focusing on using metal nanoparticles as labels, we are mainly interested in developing biological LSPR sensor systems that can be used for non-label applications. The analytical model of LSPR focuses on the physical origin of the phenomenon and its dependence on various noble metal properties. This includes the studies of spheroidal and spherical particles. The fundamental aspects of LSPR sensing, such as the description of single particles and ensembles, and comparisons of scattering, extinction, and absorption, are crucial to study. In addition, comparisons of this method with other label-free techniques are essential. The sensitivity of LSPR depends on various factors, such as nanoparticle composition, shape, dimensions, and aspect ratio. In addition, a comprehensive analysis of the literature is required to ensure that the studies are performed according to the correct standards. We classify the reports into five categories based on the biomolecular interactions that are performed. This review focuses on the various applications of LSPR for sensing chemicals, such as pH sensors and organic vapor detectors. Some of the recent developments in this area include the use of microfluidics, the multiplexing of resources, and the integration of fiber optics. The development of label-free small-scale particle and ensemble sensors (LSPRs) for molecular detection is a promising area of research. However, more studies are needed to improve the sensitivity and make them viable devices for clinical and laboratory use.

Localised Surface Plasmon Resonance

This section builds on the theoretical work behind LSPR, the supplementary material in [9] offers a significant mathematical look at plasmonics. The subsections here follow work from [10] and [11]. The work discussed in this section includes Mie theory, which is used to derive the extinction curves, Gans theory, nanoparticle fabrication, and the relationship between SPR peak wavelength and the medium's dielectric.

Theory

A plasmon refers to the collective movement of free electrons within a noble metal, essentially acting as a unit of plasma oscillation. Although the term suggests quantum mechanics, the dynamics of plasmons are accurately depicted by classical physics. These oscillations can be envisioned as the electrons moving en masse, driven by an external electric field which displaces them against the stationary positive ions of the metal. For bulk materials, where the size far exceeds the light's wavelength in all three dimensions, plasmons vibrate at what is known as the plasma frequency, possessing the energy given by [10]:

$$E_p = \sqrt{\frac{ne^2}{m\varepsilon_0}} \tag{1}$$

Here, ε_0 represents the permittivity of free space, n denotes the electron density, e signifies the electron charge, and m stands for the electron mass. Surface plasmons, also called surface plasmon polaritons (SPPs), show up at the interface of two metals. They are optically charged and can move along the surface, which is made easier by surface irregularities like gratings. The angle of incidence affects how well light and SPPs couple with each other. For best results, the incident wave vector should be almost parallel to the metal surface.

When the spatial confinement of plasmons occurs in particles of sizes on the scale of light wavelengths, namely nanoparticles, this gives rise to what is termed a localized surface plasmon (LSP). The consequential effects are twofold: a marked enhancement in the electric field in close proximity to the particle's surface, diminishing rapidly with distance, and an optical extinction peaking at the resonance frequency visible in noble metal nanoparticles. The peak's position is influenced by the refractive index of the surrounding environment, forming the foundational principle behind LSPR-based sensing techniques. A comprehensive understanding of these localized surface plasmon resonances necessitates an exploration into scattering theory which will be briefly discussed in the following subsections but detailed discussion can be found in [12].

At the surface of a metal, plasmons take the form of surface plasmon polaritons (SPPs), also simply called surface plasmons (Fig. 2). Surface plasmons are optically excited, and light can be coupled into standing or propagating surface plasmon modes through a grating or a defect in the metal surface. Because it is the oscillating electric field of the incoming plane wave that excites surface plasmons, light with a high angle of incidence (that is, with wave vector k nearly parallel to the surface) couples most efficiently.

Surface plasmon occurs when a nanoparticle is confined to a region of the electromagnetic spectrum that is similar to that of incident light. Its collective oscillation allows the free electrons of the particle to participate in the electric fields around it. The maximum optical extinction of a particle is observed at the plasmon resonance frequency, which is found in visible wavelengths. The refractive index of the medium surrounding it determines the peak of the extinction. This is the basis of the sensing applications that are being studied in this review. In order to understand how this phenomenon arises, we must first turn to scattering theory.

For a streamlined discussion, we consider a spherical nanoparticle of radius a illuminated by z-polarized light of wavelength λ, where a is significantly smaller than λ ($a/\lambda < 0.1$). In this limit, the electric field around the nanoparticle appears static, allowing us to employ a quasi-static approximation to solve Maxwell's equations. The electromagnetic (EM) field outside the particle is described by the following expression:

$$E_{\text{out}}(x, y, z) = E_0\hat{z} - \frac{\epsilon_{\text{in}} - \epsilon_{\text{out}}}{\epsilon_{\text{in}} + 2\epsilon_{\text{out}}}\frac{a^3 E_0}{r^3}\hat{z} - \frac{3z}{r^5}(x\hat{x} + y\hat{y} + z\hat{z}) \tag{2}$$

where ϵ_{in} is the dielectric constant of the nanoparticle and ϵ_{out} is that of the surrounding medium. This first term in the brackets defines the dielectric resonance condition for the nanoparticle, a critical factor for enhancing the EM field relative to the incident field.

The extinction spectrum of the nanoparticle is calculated as follows [11]:

$$E(\lambda) = \frac{24\pi^2 N a^3 \epsilon_{\text{out}}^{3/2}}{\lambda \ln(10)} \frac{\epsilon_{\text{i}}(\lambda)}{(\epsilon_{\text{r}}(\lambda) + \chi\epsilon_{\text{out}})^2 + \epsilon_{\text{i}}(\lambda)^2} \tag{3}$$

Here, ϵ_{r} and ϵ_{i} represent the real and imaginary components of the dielectric function of the metal, respectively. χ is a shape factor, taking a value of 2 for spheres and potentially larger values for particles with high aspect ratios.

Additionally, LSPR is employed for both sensing and spectroscopic applications, where the wavelength shift becomes a useful parameter. The shift in the LSPR extinction (or scattering) wavelength maximum, λ_{max}, which is sensitive to the local dielectric constant or refractive index ($\epsilon = n^2$), is governed by the presence of adsorbed species. This relationship is expressed as follows:

$$\Delta\lambda_{\text{max}} = m\Delta n\left(1 - \exp\left(-\frac{2d}{l_d}\right)\right), \tag{4}$$

where m is the bulk refractive-index response of the nanoparticle(s), Δn is the change in refractive index induced by the adsorbate, d is the effective adsorbate layer thickness, and l_d is the decay length of the EM field.

The enhancement factor for surface-enhanced Raman spectroscopy (SERS) is formulated as follows:

$$E_{\text{FSERS}}(\omega_v) = \left|\frac{E_{\text{out}}(\omega)}{E_0}\right|^2 \left|\frac{E_{\text{out}}(\omega - \omega_v)}{E_0}\right|^2$$

$$= \frac{I_{\text{SERS}}(\omega_v)}{N_{\text{surf}}} \Big/ \frac{I_{\text{NRS}}(\omega_v)}{N_{\text{vol}}} \tag{5}$$

This expression measures the Raman enhancement effect that happens when both the incident excitation and the Stokes-shifted Raman EM fields are made stronger.

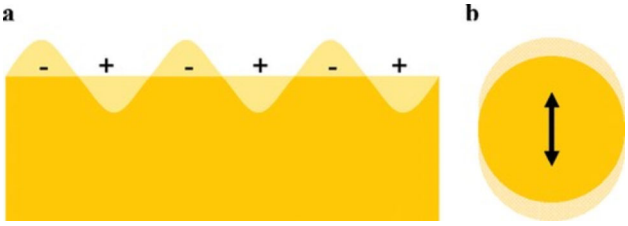

Fig. 2 Illustrations of **a** surface plasmons and **b** a localized surface plasmon. Taken from [10]

Mie Theory

Gustav Mie proposed an analytical solution to the Maxwell equations in the early 1900s, explaining how spherical par-

ticles scatter and absorb light [13]. Mie's theory can be used to determine the spectrum of various nanoparticles (NPs), as it has its foundation on Maxwell's equations [14, 15]. This theory can be used when only dipole oscillations change the extinction cross-section, C_{ext}:

$$C_{\text{ext}} = \frac{242R^3\sqrt{\epsilon_m}N\ln(10)\epsilon_i}{(\epsilon_r + \Delta\epsilon_m)^2 + \epsilon_i^2} \tag{6}$$

where R is the radius of the NP, N is the electron density, ϵ_m denotes the dielectric constant of the surrounding medium, and $\epsilon = \epsilon_r + i\epsilon_i$ represents the complex dielectric constant of the bulk metal. For spherical particles, the value of the shape-aware factor Δ in Eq. 6 is assumed to be two, but for high aspect ratio particles, such as nanorods, it may be as large as 20 [16]. The Eqs. 3 and 6 are identical to each other; in fact, they are the same equation. The coloring of the spherical NP causes the surface plasmon resonance, commonly referred to as the Fröhlich frequency, to peak at $\epsilon_r = -2\epsilon_m$. As the denominator gets closer to zero, this condition causes the electromagnetic field to intensify and the polarization to become unique. Since this condition for Ag and Au NPs occurs within the visible spectrum, these materials can be used effectively for a variety of color-based applications. Richard Gans proposed that surface plasmons for ellipsoidal NPs break into two different modes because of surface curvature and symmetry modes owing to surface curvature and symmetry [17, 18]. Theoretically, one may estimate the extinction cross-section for NPs with different forms. For instance, C_{ext} for gold nanorods can be computed as follows:

$$\sigma_{\text{ext}} = \frac{2V\sqrt{\epsilon_m}}{3}\frac{j}{(1/P_j^2)\epsilon_i}\frac{1}{(\epsilon_r + (1 - P_j/P_j)\epsilon_m)^2 + \epsilon_i^2} \tag{7}$$

where V is the particle's volume, and P_j is the depolarization factor. The depolarization factors for elongated particles are defined as follows:

$$P_{\text{length}} = 1 - \frac{e^2}{2e}\ln\left(\frac{1+e}{1-e}\right) - 1 \tag{8}$$

$$P_{\text{width}} = 1 - \frac{P_{\text{length}}}{2} \tag{9}$$

with ellipticity, e, given by the following:

$$e^2 = 1 - \left(\frac{\text{length}}{\text{width}}\right)^{-2} \tag{10}$$

Thus, ellipsoidal particles show strong, polarization-dependent spectra, where minor variations in aspect ratio lead to significant shifts in extinction bands.

For particles much smaller than the wavelength of light ($d \ll \lambda$), this theory aligns with the well-known Rayleigh scattering. The solution derives the scattered fields from a plane wave striking a homogeneous, conducting sphere, yielding the total scattering, extinction, and absorption cross-sections, represented as follows [10, 15]:

$$\sigma_{\text{sca}} = \frac{2\pi}{|k|^2}\sum_{L=1}^{\infty}(2L+1)\left(|a_L|^2 + |b_L|^2\right), \tag{11}$$

$$\sigma_{\text{ext}} = \frac{2\pi}{|k|^2}\sum_{L=1}^{\infty}(2L+1)\text{Re}(a_L + b_L), \tag{12}$$

$$\sigma_{\text{abs}} = \sigma_{\text{ext}} - \sigma_{\text{sca}}. \tag{13}$$

Here, k denotes the incoming wave vector and L are integer values denoting the dipole, quadrupole, and higher-order multipoles of the scattering process. The coefficients a_L and b_L in these equations involve Riccati-Bessel functions ψ_L and χ_L as follows:

$$a_L = \frac{m\psi_L(mx)\psi_L'(x) - \psi_L'(mx)\psi_L(x)}{m\psi_L(mx)\chi_L'(x) - \psi_L'(mx)\chi_L(x)}, \tag{14}$$

$$b_L = \frac{\psi_L(mx)\psi_L'(x) - m\psi_L'(mx)\psi_L(x)}{\psi_L(mx)\chi_L'(x) - m\psi_L'(mx)\chi_L(x)}. \tag{15}$$

In these equations, $m = \tilde{n}/n_m$, where $\tilde{n} = n_R + in_I$ is the metal's complicated refractive index, while n_m is the surrounding medium's true refractive index. Additionally, $x = kmr$, where r is the radius of the particle, and $km = 2\pi/\lambda_m$ is defined as the wavenumber in the medium, distinct from the vacuum wavenumber.

To better understand LSPR phenomena, simplified models are often more practical than Eqs. 13 to 15. Assuming the nanoparticle is much smaller than the wavelength, with $x < 1$, the Riccati-Bessel functions can be approximated by their series expansions up to x^3. According to Bohren and Huffman [15], the simplified forms for Eqs. 5 and 6 are given by the following:

$$a_1 = \frac{-i2x^3}{3\frac{m^2-1}{m^2+2}}, \quad b_1 = 0 \tag{16}$$

and higher-order terms a_L and b_L are zero, considering only terms up to x^3. For the real part of a_1 used in Eq. 3, substitute $m = \frac{n_R + in_I}{n_m}$ into Eq. 16:

$$a_1 = \frac{-i2x^3}{3}\frac{n_R^2 - n_I^2 + i2n_Rn_I - n_m^2}{n_R^2 - n_I^2 + i2n_Rn_I + 2n_m^2} \tag{17}$$

Switching to the metal's complex dielectric function $\tilde{\epsilon} = \epsilon_1 + i\epsilon_2$ with relationships:

$$\epsilon_1 = n_R^2 - n_I^2, \tag{18}$$

$$\epsilon_2 = 2n_R n_I, \tag{19}$$

and the medium's dielectric function $\epsilon_m = n_m^2$, these substitutions transform Eq. 17 to the following:

$$a_1 = \frac{2x^3}{3} \frac{-i\epsilon_1\epsilon_m + 3\epsilon_2\epsilon_m - i\epsilon_2^2 + i2\epsilon_m^2}{(\epsilon_1 + 2\epsilon_m)^2 + (\epsilon_2)^2} \tag{20}$$

Using Eq. 20 in Eq. 3 for the dipole term yields the known expression for nanoparticle plasmon resonances:

$$\sigma_{\text{ext}} = \frac{18\pi\epsilon_m^{3/2}V}{\lambda} \frac{\epsilon_2(\lambda)}{(\epsilon_1(\lambda) + 2\epsilon_m)^2 + (\epsilon_2(\lambda))^2} \tag{21}$$

where V is the particle volume. A similar process provides the scattering cross-section:

$$\sigma_{\text{sca}} = \frac{32\pi^4\epsilon_m^2 V^2}{\lambda^4} \frac{(\epsilon_1 - \epsilon_m)^2 + (\epsilon_2)^2}{(\epsilon_1 + 2\epsilon_m)^2 + (\epsilon_2)^2} \tag{22}$$

While these approximations are strictly applicable only to very small particles (diameter < 10 nm), they still accurately predict the sensitivity to dielectric changes for larger particles [19]. The sensitivity of the LSPR peak to the surrounding dielectric environment is exemplified by this dependence, and for gold particles in water ($\epsilon_m \approx 1.7$), the expected resonance wavelength where $\epsilon_1 = -2\epsilon_m$ is approximately 520 nm, consistent with experimental observations. Michael Faraday's early work on the optical properties of gold colloids highlighted the influence of particle size on color variation, setting the stage for Mie's theoretical advancements [20].

Gans Theory

While Mie's theory is tailored for spherical particles, in 1912, Richard Gans extended this to spheroidal particles under the small particle approximation [21]. He introduced the absorption cross-section for a prolate spheroid as follows:

$$\sigma_{\text{abs}} = \frac{\omega^3 c}{\epsilon_m^{3/2} V} \sum_j \left(\frac{1}{P_j^2} \epsilon_2 \left(\epsilon_1 + \frac{(1 - P_j)}{P_j} \epsilon_m \right)^2 + \epsilon_2^2 \right) \tag{23}$$

Here, P_j includes the depolarization factors P_A, P_B, and P_C, with $A > B = C$ for a prolate spheroid, affecting the dielectric values ϵ_1 and ϵ_2, and consequently the LSPR frequencies. The depolarization factors are defined as follows:

$$P_A = 1 - \frac{e^2}{2e} \ln\left(\frac{1+e}{1-e}\right) - 1, \tag{24}$$

$$P_B = P_C = \frac{1 - P_A}{2} \tag{25}$$

These equations describe how the shape and orientation of the particle affect the LSPR characteristics, highlighting the anisotropy in the plasmonic response. In this analysis, e is defined as a factor that incorporates the particle's aspect ratio R, given by the following:

$$e = 1 - \sqrt{1 - \left(\frac{B}{A}\right)^2} = 1 - \frac{1}{\sqrt{R^2}} \tag{26}$$

The extinction spectrum described by Eq. 19 exhibits two distinctive peaks: one arising from the transverse plasmon mode due to the x and y components, and the other from the longitudinal plasmon mode due to the z component. This model not only sheds light on the plasmon resonance modes but also clarifies how the aspect ratio impacts the LSPR peak wavelength. Specifically, the weighting factor for ϵ_m, which is 2 for spherical particles, becomes $\left(\frac{1-P_j}{P_j}\right)$, a value that increases with the aspect ratio and typically exceeds 2. This increase results in a red shift of the plasmon peak and heightens the sensitivity to the surrounding medium's dielectric constant.

For shapes beyond spheres and spheroids, the influence of particle morphology on the LSPR spectrum becomes significant, albeit challenging to describe analytically. Instead, numerical simulations such as the finite difference time domain (FDTD), discrete dipole approximation (DDA), and finite element method (FEM) are essential. A comprehensive review by Zhao et al. [22] provides an introduction to these methods.

Alternative and Emerging Techniques Other techniques include the economical nanosphere lithography (NSL), which creates metal films over nanosphere structures and 2D periodic arrays. These structures are highly efficient for surface-enhanced Raman scattering (SERS) due to their rough surfaces. In the NSL process, polymer nanospheres self-assemble into a hexagonal pattern, which is subsequently coated with metal. Once the mask is removed, it leaves behind a honeycomb lattice of triangular islands, the size of which can be adjusted by the sphere's spacing. Other methods used to make nanoparticles are laser ablation and electrodeposition, which give scientists a lot of ways to change the shape and plasmonic properties of nanoparticles. Techniques like focused ion beam milling are preferred for their reliability and have been widely adopted for creating precise nanohole arrays and other complex nanostructures.

Relationship Between SPR Peak Wavelength the Medium's Dielectric

To find out how the dielectric function of the medium affects the LSPR peak wavelength, the Drude model gives an analytical form for (ϵ_1) that changes with frequency and describes the electronic structure of metals.

$$\epsilon_1 = 1 - \frac{\omega_p^2}{\omega^2 + \gamma^2} \tag{27}$$

Here, ω_p is the plasma frequency, and γ is the damping factor for the metal. In the visible to near-infrared spectrum, where $\gamma \ll \omega_p$, this expression simplifies to the following:

$$\epsilon_1 = 1 - \frac{\omega_p^2}{\omega^2} \tag{28}$$

Setting $\epsilon_1 = -2\epsilon_m$ (resonance condition), the LSPR peak frequency $\omega_{\max}$ is derived as follows:

$$\omega_{\max} = \omega_p \sqrt{2\epsilon_m + 1} \tag{29}$$

Converting frequency to wavelength λ using $\lambda = \frac{2\pi c}{\omega}$, and relating dielectric constant to refractive index with $\epsilon_m = n_m^2$, we obtain the following:

$$\lambda_{\max} = \frac{\lambda_p}{\sqrt{2n_m^2 + 1}} \tag{30}$$

where $\lambda_{\max}$ is the LSPR peak wavelength, and λ_p is the wavelength associated with the plasma frequency of the metal. Experimental results suggest that the dependence of the LSPR peak wavelength on the refractive index is approximately linear within optical frequencies, as depicted in Eq. 30.

Fabrication of Nanostructures for LSPR

For LSPR, stable metal nanoparticles such as Au, Ag, and Pt/Pd work well and can be used to improve biosensing's sensitivity, selectivity, and low interference. The stability of metal nanoparticles and LSPR effectiveness response depends on the synthesis method and nanoparticles arrangement, while the synthesis method influences the nanoparticle size [24]. Metal nanoparticles such as Au, Ag, Pt/Pd, and Ti are the most stable for LSPR, and different techniques have been used to date to synthesize them (Table 1). These nanoparticle metals have been used intensely to study the interaction between molecules and localized surface plasmons when the light of a certain wavelength passes through [25]. The size, shape, and arrangement of nanoparticles are significant factors in LSPR. For example, Au nanoparticles can take on various morphologies, such as spherical- and nanorod-shaped. Figure 3 shows how each morphology is created using a particular process, and characterization methods like UV–Vis spectroscopy can be used to determine the stability and changes that cause individual nanoparticles to aggregate into clusters that change in size, shape, and interparticle distance [26].

Table 1 Metal nanoparticle synthesis methods

Material	Synthesis methods
Gold	• Vapor transport
	• Citrate reduction
	• Citrate reduction: Deposition of Au nanoparticles on Tellurium nanowire surface [27]
	• Reduction using $NaBH_4$ Au precursor
Silver	• Citrate reduction of silver precursor with ascorbic acid
	• Citrate reduction
	• AC electrodeposition of synthesized Ag nanowires in ordered aluminum oxide surface [28]
Platinum (Pt)	• Electrodeposition of Pt onto conducting surface using polystyrene latex spheres
	• Reduction of H_2PtCl_6 with either ascorbic acid, sodium borohydride, or sodium citrate [29]
	• Au nanoparticles: Citrate reduction of $HAuCl_4$ followed by reduction of H_2PtCl_6 with ascorbic acid to synthesize Pt

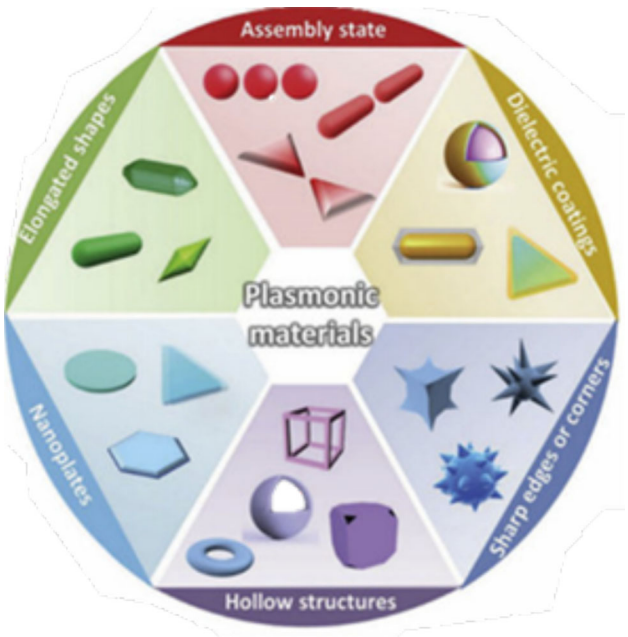

Fig. 3 An example of the wide range of metallic nanoparticle morphologies that are currently achievable, reproduced from the work by Zhu et al. with permission from the Royal Society of Chemistry Copyright (2014) [23]

The formation, shape, and size of nanoparticles generated for LSPR may currently be evaluated using a wide range of characterization techniques; these characteristics dictate a nanoparticle's potential and application [30]. Techniques for characterizing materials aid in determining their dimensions, morphological surfaces, and enhanced comprehension of the composition and structure of materials. Table 2 shows different techniques applied to understanding nanoparticle properties.

The creation of nanostructures for localized surface plasmon resonance (LSPR) utilizes both top-down and bottom-up fabrication techniques [31]. Generally, bottom-up methods are employed in semiconductor quantum dot self-assembly. In contrast, top-down techniques are typically used in the creation of gold (Au) and silver (Ag) nanostructures. This section goes over the different fabrication methods for nanoparticles [28].

Wet Chemical Reduction Method [37–39] Noble metals usually crystallize as face-cantered cubic; single crystal nanoparticles take on the shape of a Wulff polyhedron, which is a truncated octahedron. Different shaped nanoparticles can be formed during synthesis by adding stabilizing agents and surfactants. One popular method for manipulating the shape of nanoparticles is seed-mediated synthesis. The final nanoparticle structure is determined by the properties of the seed, such as twinning defects or stacking faults. These defects enhance the reactivity at specific sites, guiding the growth toward certain shapes such as octahedrons or cubes, and further facilitating the development of nanorods and nanobars.

Nanoparticle synthesis generally involves a two-stage process. Initially, rapid nucleation occurs when a metal precursor is reduced to form seed particles, typically ranging from 1 to 5 nm in size, under high precursor concentration conditions. It takes longer for these seeds to mature into larger nanoparticles since more metal ions must be added gradually, and frequently a different reduction agent is needed. For instance, gold nanoparticles are commonly produced by reducing gold chloride with sodium citrate in a heated aqueous solution, while silver nanoparticles are synthesized using silver nitrate with sodium borohydride or sodium citrate. The choice of capping agents, which bind selectively to particular crystal facets to direct the growth, affects the growth dynamics.

In this method, noble metals form face-centered cubic crystals, typically crystallizing into single-crystal nanoparticles known as Wulff polyhedrons. The addition of surfactants and stabilizers during the synthesis process enables the creation of nanoparticles in diverse shapes. Seed-mediated synthesis is a crucial technique here, as the characteristics of the initial seed, like twinning defects or stacking faults, influence the final shape of the nanoparticles. The synthesis typically starts with the rapid nucleation of metal nuclei through the reduction of a metal precursor, forming seed particles. This is followed by a slower phase where these seeds grow into larger nanoparticles as more metal ions are added, often with a different reducing agent. The reduction of gold chloride by sodium citrate in a hot aqueous solution is a standard method for producing gold nanoparticles, while silver nanoparticles are typically synthesized using silver nitrate and sodium

Table 2 Different characterization techniques and their roles

Role of the characterization technique	Characterisation technique
Identification of morphological surfaces, including crystalline or amorphous surfaces with uniform or imperfections on the surfaces, such as spherical, flat, cylindrical, tubular, conical, and irregular shapes [32]	Scanning electron microscopy, transmission electron microscopy, and atomic force microscopy
Measurement of the size distribution and surface charge/zeta potential of molecules and particles, usually in the submicron range [33]	Dynamic light scattering
The analysis of the chemical or elemental makeup establishes the nanoparticle's performance and purity [32]	X-ray photoelectron spectroscopy and energy-dispersive X-ray spectrometry
Determination of crystallography of the nanoparticles [34, 35]	X-ray powder diffraction
Determination of the concentration, and chemical light absorbance measurement [36]	UV–Vis absorption spectroscopy

borohydride or sodium citrate. The influence of various capping agents is significant as they bind to specific crystal facets and control the growth direction.

Lithography and Vapor Deposition Vapor deposition methods, including vacuum deposition and sputtering, are widely used to create ultra-thin metallic nanoislands. These methods produce films with thicknesses less than 10 nm by vaporizing a metal and letting the metal atoms condense. Such instruments like a quartz crystal microbalance are used to monitor this process. Various lithographic processes are used to produce nanopatterned structures such as dimers, periodic particle arrays, and nanoholes. Electron beam (EB) lithography, in particular, offers precise control over the size, shape, and distribution of nanostructures, achieving high monodispersity due to its resolution capabilities, which can be less than 100 nm. Typically, a conductive film-coated glass slide is covered with an electron-sensitive photoresist, like poly(methyl methacrylate) (PMMA), to achieve these detailed nanopatterns. Nanofabrication for LSPR employs both top-down and bottom-up approaches. These methods are used to produce ultra-thin metallic nanostructures. Techniques like vacuum deposition or sputtering involve the evaporation of metal, which then condenses to form nanoislands with precise thickness, monitored via a quartz crystal microbalance. Nanopatterns such as periodic particle arrays and nanoholes are crafted using lithographic methods.

Nanoimprint Lithography (NIL) Considered a next-generation technique, NIL offers high precision similar to EB lithography but with the throughput suitable for large-scale applications. In traditional methods, photons or electrons are used to change a resist. NIL, on the other hand, mechanically molds the polymer material, which lets very fine structures be made based on the design of the imprinting stamp.

Kinetics Studies in LSPR Biosensing

Localized surface plasmon resonance biosensing is a powerful technique for studying the kinetics of biomolecular interactions in real-time. The following section outlines the key equations used in LSPR kinetic studies and provides a brief overview of the process [40].

Theoretical Background

The kinetics of biomolecular interactions in LSPR biosensing can be described using the Langmuir adsorption model. This model assumes that the binding of analyte molecules to the sensor surface is reversible and can be represented as follows:

$$A + B \rightleftharpoons AB, \tag{31}$$

where A represents the analyte, B the binding sites on the sensor surface, and AB the analyte-bound complex.

Rate Equations

The association and dissociation of the analyte to the sensor surface can be described by the following rate equations:

$$\frac{d[AB]}{dt} = k_a[A][B] - k_d[AB], \tag{32}$$

where k_a is the association rate constant, k_d is the dissociation rate constant, $[A]$ is the concentration of the analyte, $[B]$ is the concentration of free binding sites, and $[AB]$ is the concentration of the bound complex. At equilibrium, the rate of association equals the rate of dissociation:

$$k_a[A][B] = k_d[AB] \tag{33}$$

Kinetic Analysis

By integrating the rate equations, we obtain the following expressions for the association and dissociation phases:

Association Phase

During the association phase, the concentration of the bound complex $[AB](t)$ as a function of time t is given by the following:

$$[AB](t) = [AB]_{\max}\left(1 - e^{-(k_a[A]+k_d)t}\right) \tag{34}$$

where $[AB]_{\max}$ is the maximum concentration of the bound complex.

Dissociation Phase

During the dissociation phase, when the analyte is removed from the solution, the concentration of the bound complex decreases according to the following:

$$[AB](t) = [AB]_{\max}e^{-k_d t} \tag{35}$$

Data Fitting and Parameter Extraction

To extract the kinetic parameters k_a and k_d from experimental data, nonlinear curve fitting techniques are employed. The following expressions are fitted to the sensor response curves obtained during the association and dissociation phases:

Association Phase

For the association phase:

$$R(t) = R_{\max}\left(1 - e^{-(k_a[A]+k_d)t}\right) \tag{36}$$

Dissociation Phase

For the dissociation phase:

$$R(t) = R_{\max}e^{-k_d t} \tag{37}$$

where $R(t)$ is the sensor response at time t, and $R_{\max}$ is the maximum sensor response.

Sensing Metrics with LSPR

Refractive Index Sensing

LSPR-active particles are primarily utilized to detect changes in the refractive index of the environment by monitoring shifts in the LSPR peak wavelength. These shifts are usually detected through either spectral extinction measurements in dense films or spectral scattering measurements in single NPs. The differences in these measurement approaches are illustrated in Fig. 4, which presents spectra of three different nanoparticle shapes, all set on glass substrates in air.
For small gold nanorods, the ensemble extinction spectra exhibit two prominent peaks corresponding to the transverse and longitudinal modes. However, in single-particle measurements, scattering is generally too faint to detect due to the dominance of absorption. In contrast, larger nanorods exhibit more significant scattering, which can be readily measured. Ensemble measurements of gold nanostars are very different from single-particle measurements. Ensemble measurements usually show a broad peak that includes many overlapping spectra, while single-particle measurements show clear peaks for each nanostar arm, which shows how they are structured differently. With gold bipyramids, the ensemble extinction again shows distinct peaks, but single-particle scattering highlights a clear peak specifically from the bipyramids. This variability underscores the methodological choice between ensemble extinction for smaller particles and single-particle scattering for larger, more brightly scattering particles. The LSPR peak wavelength's shift tends to follow an approximately linear relationship with changes in the refractive index of the surrounding medium. The sensitivity is a measure of how much the LSPR peak wavelength changes when the refractive index changes Eq. 38: in nanometers per refractive index unit (nm/RIU)

$$S = \frac{d\lambda_p}{dn} \tag{38}$$

An example of this sensing capability is demonstrated in [10] (Fig. 7 of that paper) using a gold nanorod film exposed to various solvents with different refractive indices: air ($n = 1.000$), water ($n = 1.333$), ethanol ($n = 1.361$), and formamide ($n = 1.428$). Though not perfectly linear, the relationship between the plasmon resonance wavelength and the refractive index approximates linearity well over small ranges of n. The precision of LSPR sensing, influenced by the sensitivity S and the resonance line width, leads to a commonly used metric called the figure of merit (FOM), which is the sensitivity divided by the resonance line width:

$$FOM = \frac{S}{\Delta\lambda} \tag{39}$$

The figure of merit helps evaluate the efficacy of a nanoparticle's sensing capabilities, highlighting the trade-off between sensitivity and spectral resolution.
The analysis of LSPR spectra often includes the resonance energy shift, typically expressed in electron volts (eV). Both nm/RIU and eV/RIU units are used in our comparative tables of nanoparticle sensitivities. It is worth noting that the LSPR shift is not strictly linear with the refractive index n in either measurement unit, as shown in Eq. 30. When converting this equation to energy units, the relationship between energy E and n is given by the following:

$$E = \frac{hc}{\lambda_p\sqrt{2n_m^2 + 1}} \tag{40}$$

Although there is some non-linearity, within the narrow spectral range typically probed in experiments, the LSPR shift approximates linearity at visible frequencies. Recently, Becker et al. introduced a new figure of merit, termed FOM*, which serves as a generalized metric for comparing the sensing capabilities of different nanostructures. This is particularly useful for complex plasmonic structures like metamaterials, where defining a consistent line width $\Delta\lambda$ is challenging. FOM* is defined without incorporating the line width, focusing instead on the relative intensity change $\frac{dI}{I}$ at a specific wavelength λ_0 upon a slight change dn in the local refractive index:

$$\text{FOM}^* = \left(\frac{dI}{dn}\cdot\frac{1}{I_0}\right)_{\max} = \left(\frac{dI}{d\lambda}\cdot\frac{d\lambda}{dn}\cdot\frac{1}{I_0}\right)_{\max} \tag{41}$$

$$= \left(S\cdot\frac{dI}{d\lambda}\cdot\frac{1}{I_0}\right)_{\max} \tag{42}$$

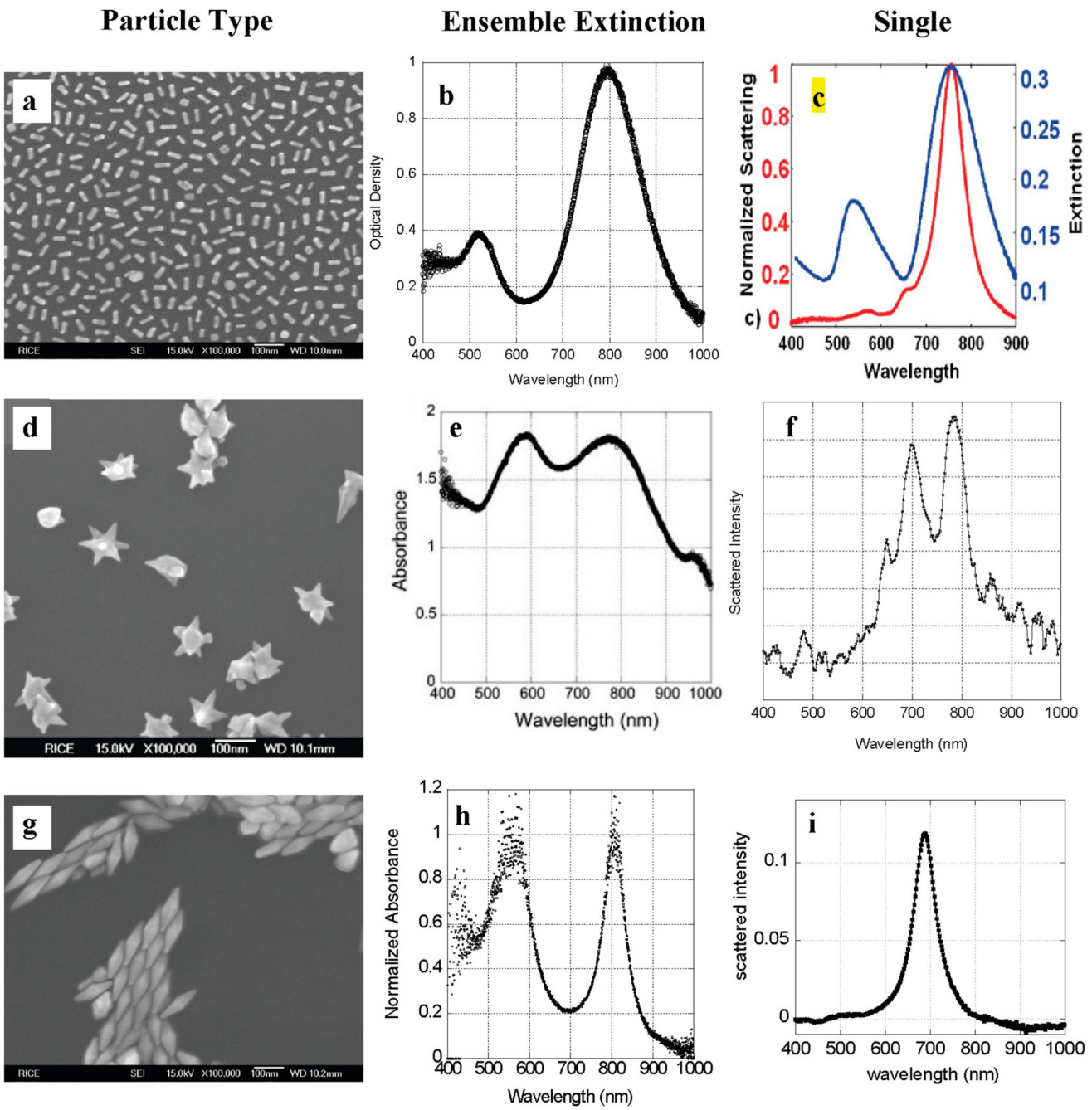

Fig. 4 Figure 6 shows a comparison of the extinction spectra for three different particle types, both as an ensemble and as single-particle scattering. Gold nanorods. **b** Extinction of a nanorod ensemble. The two peaks are associated with the transverse and longitudinal plasmon modes of the particle. The nanorods depicted in **a** and **b** have a scattering intensity that is too low to acquire spectra for individual particles. However, larger nanorods may exhibit measurable scattering. Gold nanostars. **e** Extinction of nanostar ensembles. Particle spectra are spread out and combined into a wide peak in the near IR. **f** Spectrum of single-particle scattering by a nanostar. There are several peaks in the near IR that align with the resonances of the star's arms. Gold bipyramids. **h** Extinction of the bipyramid ensemble. There are two peaks that can be seen, which can be attributed to bipyramids and spheres. **i** Scattering spectrum of a single particle in the shape of a bipyramid. There is a solitary, intense spike visible. The wavelength at which it occurs is different from **h** due to the particle originating from a separate batch, resulting in a distinct aspect ratio of gold bipyramids. Taken from [10]

This metric is defined at the wavelength where the maximum intensity change occurs with respect to the refractive index. FOM* can also be expressed using the refractive index sensitivity S in nm/RIU, as shown in the final expression

of Eq. 41. Figure 10 in [10] contrasts FOM and FOM* for gold nanorods with different aspect ratios. The peak FOM is observed for nanorods with an aspect ratio of 4.3, optimal for applications involving LSPR spectral peak fitting, while the highest FOM* is seen in nanorods with a slightly lower aspect ratio of 4.2, suitable for applications focusing on intensity changes at a fixed wavelength.

Another crucial parameter for assessing the efficacy of an LSPR sensor is the quality factor [41], denoted as Q-factor, which is significantly impacted by absorption attributed to a high imaginary part of the dielectric constant, ϵ. A broader resonance results in a lower Q-factor, indicating that the bandwidth of the resonance provides a measure of the resonance's strength and compactness. The Q-factor is mathematically defined as follows:

$$Q = \frac{\lambda_{\text{central}}}{\text{FWHM}}$$

where λ_{central} is the central wavelength of the plasmon resonance. Ru et al. [42] have also provided a comparison of Q-factors for the most commonly used metals, as illustrated in Fig. 5. Another significant attribute is the spectral resolution, typically defined as the minimum detection limit. Unlike traditional SPR sensors, the resolution of LSPR sensors can be enhanced by adjusting the size and geometry of the nanoparticles. These linked factors critically describe the sensing performance and are employed to evaluate various types of sensors throughout this review.

Molecular Sensing

LSPR sensors are highly effective not only for detecting shifts in the bulk refractive index, which is useful for calibration, but also for their capacity to sense at a localized scale. The field enhancements associated with LSPR rapidly diminish with increasing distance from the nanoparticle surface. Consequently, spectral LSPR shifts primarily interrogate a nanoscale region adjacent to the particle. This focused sensing zone lets us see how molecules interact with the nanoparticle surface by looking at changes in the local refractive index, as shown in Fig. 6, which shows the difference between bulk and molecular LSPR sensing.

One exemplary application of molecular sensing via LSPR is the formation of self-assembled monolayers (SAMs) on nanoparticle surfaces. SAMs, particularly those composed of alkane thiols, are a well-established method for modifying the surfaces of gold and silver nanostructures. Malinsky et al. and Haes et al. showed how useful this method is by measuring the LSPR shift caused by monolayer formation on silver nanotriangles. This process clearly shows how the nanoparticles can sense their surroundings [43, 44].

Molecular Sensing via Lithography

Utilizing lithography, researchers have employed self-assembled monolayers (SAMs) with progressively increasing carbon chain lengths to monitor LSPR shifts induced by the addition of each CH_2 group. Furthermore, these studies have

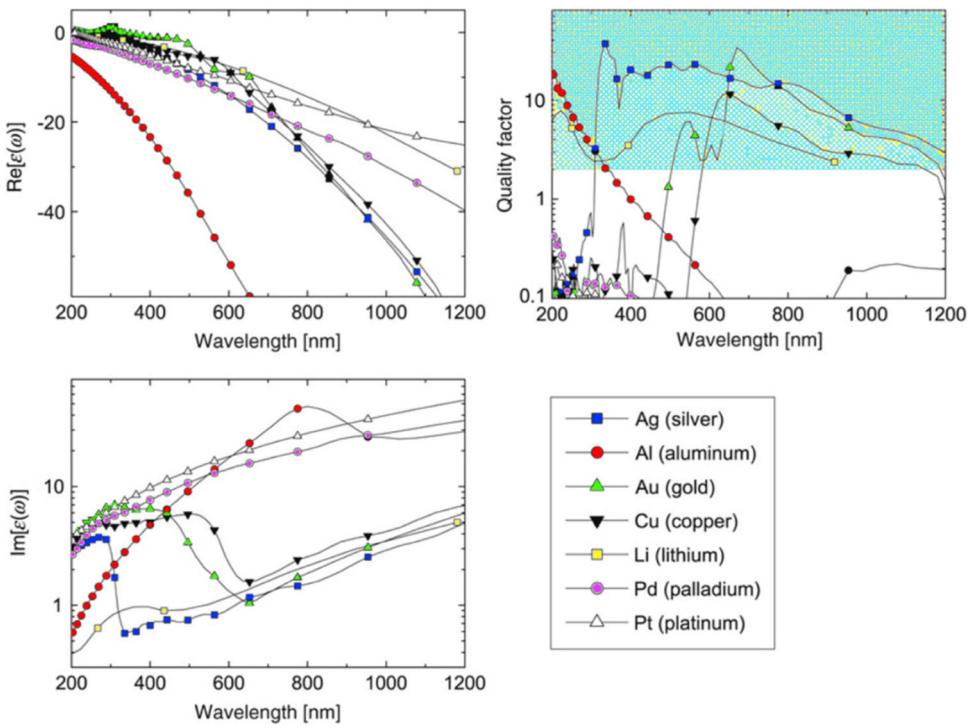

Fig. 5 A selection of metals' optical properties. Real (top) and imaginary (bottom) components of ϵ are plotted against wavelength on the left. Also depicted (top-right) is the approximate Q-factor of LSPR for a metal/air NP interface. For numerous plasmonics applications, the shaded region is of particular interest. Taken from [28]

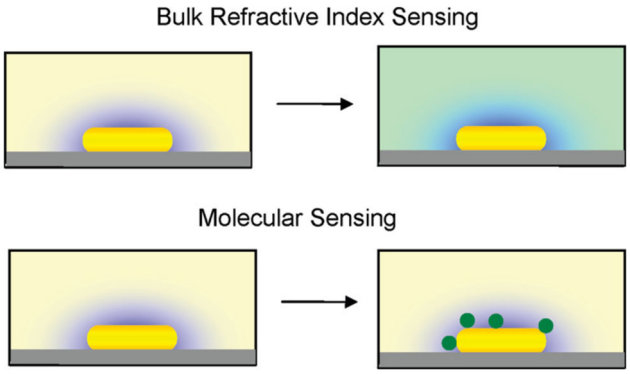

Fig. 6 Comparison of molecular sensing via LSPR with bulk refractive index sensing. The dielectric environment of the particle changes only in the latter situation within the sensing volume. Taken from [10]

documented how LSPR sensitivity decreases as the distance from the surface increases, using SAMs of extended chain lengths. As depicted in Fig. 12a, SAMs ranging from 2 to 17 carbon atoms exhibit a linear relationship between LSPR peak wavelength and layer thickness up to a distance of 3 nm from the nanoparticle surface. In a subsequent experiment shown in Fig. 12b, alternating layers of SAMs and copper ions were deposited to create multilayer structures extending from 2 to 34 nm from the surface. Here, the LSPR shift per added layer stabilizes for layer thicknesses beyond approximately 20 nm.

These findings are crucial for biosensor design, suggesting that the thickness of the capture layers should be kept below 20 nm to ensure observable shifts due to target binding. This also underscores the importance of distinguishing between a nanoparticle's bulk refractive index sensitivity, which is highly dependent on the particle's surface structure and surrounding circumstances, as well as its molecular detection sensitivity.

Nusz et al. proposed a unique figure of merit for assessing the molecular detection sensitivity of nanoparticles, termed $\mathrm{FOM_{mol}}$ [45]. $\mathrm{FOM_{mol}}$ is defined as the ratio of the maximum number of bound molecules (dynamic range, DR) to the minimum detectable molecules (molecular detection limit, MDL):

$$\mathrm{MDL} = \frac{V_S}{\sqrt{U_{\mathrm{system}}^2 + U_{\mathrm{fit}}^2}} \cdot \frac{V_A \Delta R I e^{-2r/\lambda_d} S_0}{3}. \tag{43}$$

Here, V_S is the sensing volume, V_A the analyte volume, ΔRI the refractive index difference between the analyte and the surrounding medium, U_{system} the system uncertainty in detecting the LSPR peak, U_{fit} the fitting uncertainty of the LSPR peak, S_0 the bulk refractive index sensitivity, r the distance from the particle surface to the analyte binding site, and λ_d the decay length of the electric field from the particle surface.

For gold nanorods, it was determined that the ideal dimensions for molecular detection of streptavidin are approximately 60 nm by 30 nm, with a predicted MDL of 18. Becker et al. also analyzed nanorod geometries and suggested that optimal sensing occurs with an aspect ratio between 3 and 4 [46]. Furthermore, Becker et al. introduced another figure of merit for thin layers, defined as follows:

$$\mathrm{FOM_{layer}} = \left(\frac{dI}{I}\frac{dl}{1}\right)_{\mathrm{max}}, \tag{44}$$

where I is the initial intensity at the wavelength experiencing the maximum intensity change with the refractive index. While the $\mathrm{FOM_{mol}}$ uses a simplified model that does not account for spatial variations in sensitivity, it provides significant insights into factors influencing molecular detection sensitivity beyond bulk refractive index sensitivity.

Effects of Particle Size, Shape, and Material

Nanoparticle Size and Aspect Ratio

The LSPR properties of metal nanoparticles are heavily dependent on the particle's size. According to Mie's theory, for spherical nanoparticles with a radius R significantly smaller than the wavelength of light ($2\pi R < \lambda$), the scattering cross-section scales with R^6 while absorption scales with R^3. As a result, LSPR extinction in smaller particles is predominantly due to absorption, but as particle size increases, scattering becomes more prevalent. For instance, in gold nanospheres, the transition from absorption to scattering dominance occurs around a particle diameter of 80 nm. Moreover, the LSPR wavelength itself can be adjusted over a range of 60 nm by varying the particle size from 10 to 100 nm, a phenomenon first observed by Richard Zsigmondy in 1909 during early dark field microscopy studies of gold colloids (see Fig. 7). The resonance line width also varies with size, influenced by interband transitions and higher-order plasmon modes, which respectively increase line width in smaller and larger particles.

Furthermore, for spheroidal particles, refractive index sensitivity depends not just on the material and size, but also on the aspect ratio. For example, experiments with gold nanorods of 10 nm radius demonstrated that sensitivity increases from 157 to 497 nm/RIU as the aspect ratio increases from 1.0 (spherical) to 3.4. Similarly, gold bipyramids have shown sensitivity increases from 150 to 540 nm/RIU as the aspect ratio increases from 1.5 to 4.7, even as particle radius varied.

Nanoparticle Shape

Nanoparticle shape has a considerable (Figs. 8 and 9) influence on the LSPR's sensitivity of non-spheroidal particles,

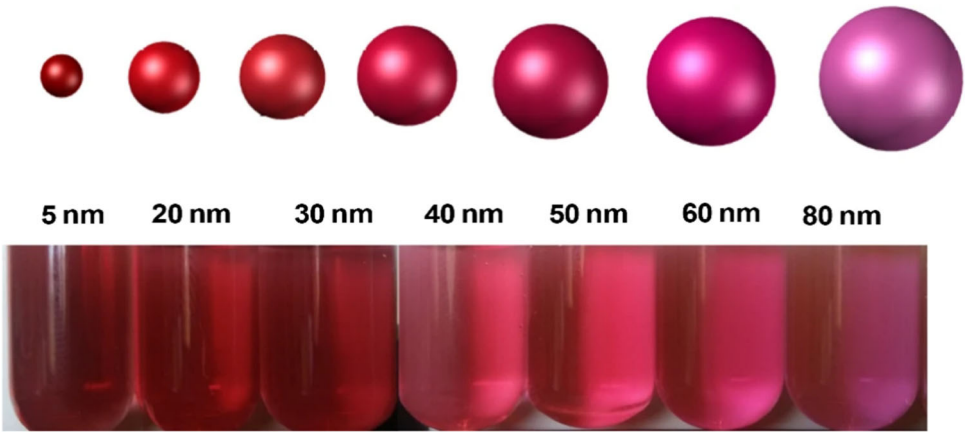

Fig. 7 This image shows old nanoparticle colloidal suspensions of colloidal gold nanoparticles taken over a range of sizes (the size of the colloids run from 5–80 nm). Taken from [47]

which cannot be anticipated analytically, as shown by electrodynamic simulations and tests. Notably, particles with sharp features, such as tips, exhibit much higher refractive index sensitivities than those predicted by their aspect ratios alone. This has led to the development of various new nanoparticle shapes designed to enhance refractive index sensitivity. For instance, Mock et al. compared silver nanoparticles of different shapes (spheres, triangles, cubes) of similar volume and found that nanotriangles exhibited significantly higher sensitivity (350 nm/RIU) compared to spheres (160 nm/RIU). Additionally, Sun et al. [48] observed that gold nanospheres and nanoshells of the same dimension differed significantly in sensitivity, with the nanoshells exhibiting significantly better sensitivity (409 nm/RIU vs. 60 nm/RIU). Sharp particles not only move the plasmon resonance to lower energies, which makes the refractive index more sensitive, but they also create localized modes with very strong electric fields, which is good for finding molecules. This effect was seen in many studies, such as those that used silver nanocubes and gold bipyramids. In these studies, sharp features caused big red shifts in plasmon resonance, which made the sensors more sensitive. These observations underscore the complex interplay between particle shape, size, and material composition in determining LSPR properties and their potential applications in biosensing.

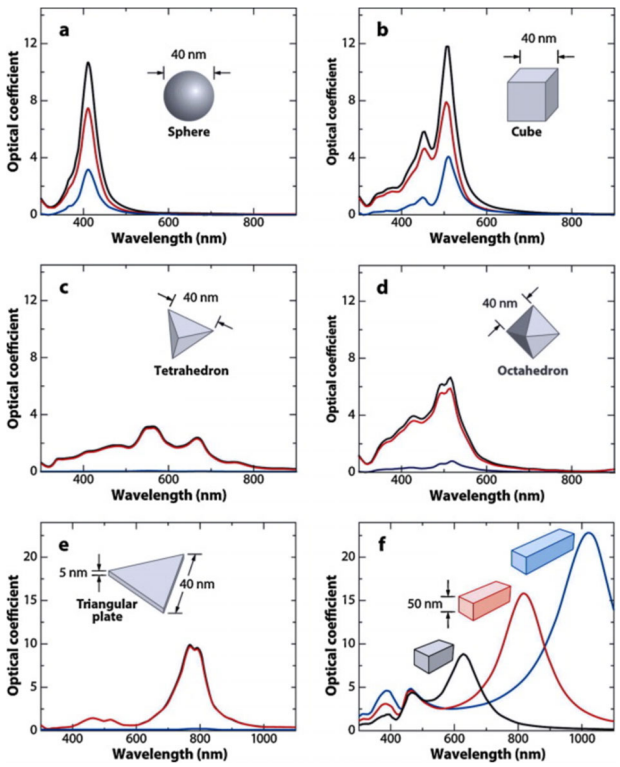

Fig. 8 The extinction (represented in black), absorption (shown in red), and scattering (depicted in blue) spectra have been computed for silver nanoparticles of various shapes: **a** a sphere, which shows a single dipole resonance peak, and other shapes including **b** a cube, **c** a tetrahedron, **d** an octahedron, and **e** a triangular plate. Additionally, **f** illustrates the extinction spectra for rectangular bars with aspect ratios of 2 (black), 3 (red), and 4 (blue). Typically, these nonspherical nanoparticles display several resonance peaks, which are shifted towards the red end of the spectrum. Taken from [28]

Nanoparticle Material

The majority of LSPR sensing studies utilize gold or silver nanoparticles. Gold is favored for its chemical stability and oxidation resistance, whereas silver nanoparticles are preferred for their sharper resonances and enhanced refractive index sensitivity. These distinctions are demonstrated by a direct comparison of silver and gold nanoparticles that retain comparable sizes and shapes. As an example, spheres with a diameter of 50–60 nm show refractive index sensitivity of 60 nm/RIU for gold at a plasmon resonance of about 530 nm, and 160 nm/RIU for silver at about 435 nm. Comparably, nanocubes with sizes ranging from 30 to 50 nm have a sensitivity of 83 nm/RIU for gold at 538 nm and 146 nm/RIU for silver at 510 nm (see Figure 25 and Table 3 in [10]). Despite the shorter plasmon resonance wavelengths of silver, these

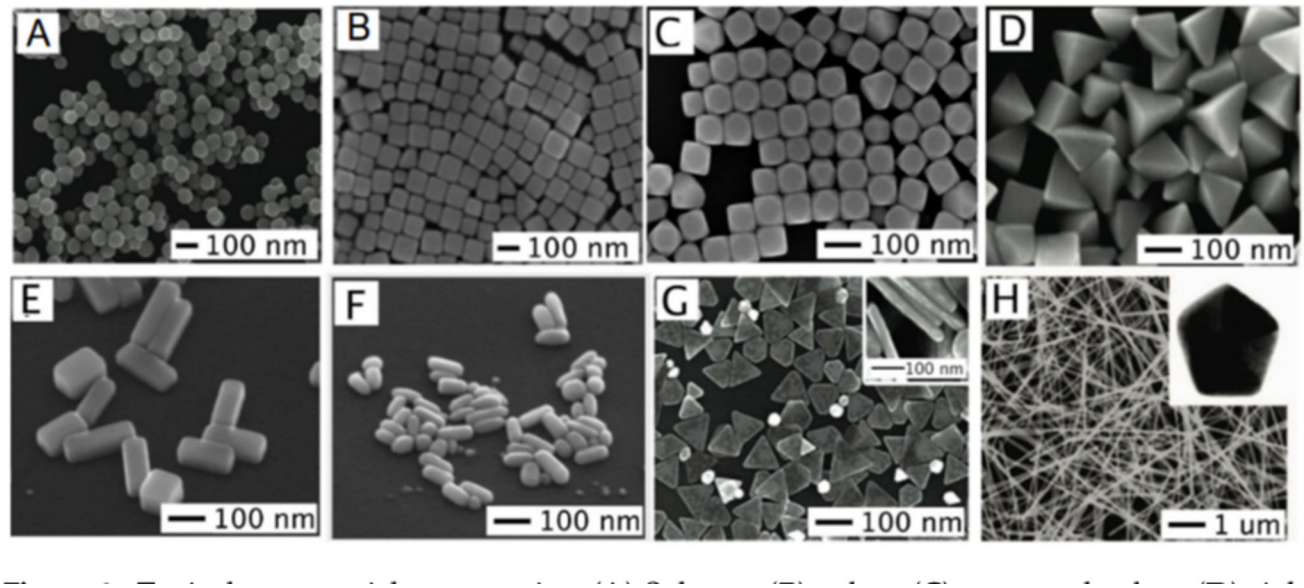

Fig. 9 Standard nanoparticle shapes include the following: **A** spheres, **B** cubes, **C** truncated cubes, **D** right nanobipyramids, **E** bars, **F** spheroids, **G** triangular plates, and **H** wires. Reproduction is authorized. Taken from [41]

nanoparticles display higher sensitivity than their gold counterparts due to the intrinsic properties of the materials.

The underlying reasons for these differences are rooted in the metals' dielectric functions. The peak position of plasmon resonance for spherical nanoparticles is determined by the wavelength where $\epsilon_1 = -2\epsilon_m$. Silver's real dielectric function changes more significantly over the visible spectrum, particularly between 400 and 600 nm, which typically encompasses the plasmon resonance range for common dielectric constants. Moreover, silver exhibits less plasmon damping due to a lower imaginary part of its dielectric function across the visible spectrum, resulting in higher scattering efficiency and narrower plasmon linewidths. This makes silver nanoparticles particularly advantageous for practical sensing applications, providing sharper and more distinct plasmon resonance peaks that facilitate more precise measurements.

Link et al. [49] further explored these differences through experiments on nanoparticles made from gold-silver alloys of varying compositions. They demonstrated that the material composition affects the plasmon peak wavelength more so than particle size. They found a linear relationship between the plasmon peak wavelength and the amount of gold in the alloy. Beyond silver and gold, plasmonic nanoparticles can also be synthesized from other metals such as palladium, which have been formed into shapes like nanocubes, prisms, and plates with tunable plasmon resonances ranging from 330 to 530 nm. However, the potential sensing applications of these palladium nanoparticles remain largely unexplored [49].

LSPR Dependence on NP Morphology, Distance Separation, and Proximity to NPs

The influence of NP morphology on LSPR is significant, particularly due to changes in surface polarization triggered by variations in shape and size [28]. Different shapes like spheres, triangles, cubes, and more complex structures such as nanorods and nanostars have been engineered to modify LSPR absorption across the visible-to-infrared spectrum. Sharper or more angular NP shapes tend to shift the extinction spectra towards the red due to enhanced charge separation, while a more symmetrical shape intensifies LSPR signals. The potential for a nanoparticle to exhibit multiple absorption peaks correlates with its ability to support various polarization modes.

For example, nanorods, which can be polarized along both transverse and longitudinal axes, demonstrate dual LSPR peaks. Particle size also affects the absorption and scattering cross-sections, with smaller NPs predominantly absorbing light, and larger ones scattering more [28]. This size-dependent behavior impacts the scattering-to-absorption ratio, which generally remains constant regardless of the NP's aspect ratio. Deviations from spherical shapes influence LSPR more than mere size changes. For instance, enlarging a spherical NP from 10 to 100 nm induces a 47 nm red shift, whereas changing the aspect ratio of an elliptical NP from 2.5 to 3.5 causes a 92 nm shift in the longitudinal band. Nanoparticle's shapes, particularly those like nanorods and triangles, also affect refractive index sensitivities, which are crucial for applications like surface-enhanced spectroscopy.

This sensitivity and the accompanying spectral shifts are due to the "lightning rod effect," where electromagnetic fields are intensified at sharp tips or edges.

Additionally, the dielectric sensitivity of NPs, which is vital for their responsiveness to environmental changes, depends on their LSPR spectral positioning and physical shape. Studies have shown varying shifts in spectral response based on NP morphology and surrounding media. The distance between particles is also very important, especially when the particles are arranged in dimers or aggregates, because electromagnetic interactions between them can make the LSPR effects stronger. LSPR responses depend a lot on the shape, size, and proximity of nanoparticles to each other or to adsorbates. These factors affect the spectral properties and possible uses of NPs in areas such as sensing and spectroscopy.

Significant efforts in nanomaterials research have focused on shifting the LSPR band from the visible (VIS) to the near-infrared (NIR) spectrum. Metals such as gold (Au), silver (Ag), copper (Cu), and aluminum (Al) efficiently reflect light at VIS wavelengths due to the presence of free conduction electrons, which influence both optical and other physical properties like thermal and electrical conductivity. It is well-documented that as these metals approach NIR wavelengths, the real part of their permittivity increases, posing a challenge for their use in NIR-based plasmonic sensors. The complex permittivity of these metals up to wavelengths of 3 μm has been characterized, showing both real and imaginary components. It is important for plasmonic applications, especially LSPR, that the metals have a negative real permittivity (ϵ') in the right range, ideally between -20 and -1, along with a small imaginary permittivity (ϵ''), which means they have a high Q-factor (ideally greater than 10). Metals like aluminum are less favored for NIR plasmonics due to their high ϵ'. Metals such as palladium, platinum, and lithium, despite their other properties, are also unsuitable due to high absorption and reactivity with water. Gold stands out due to its superior corrosion resistance, a crucial factor distinguishing it from copper. Practical considerations such as availability, ease of manipulation, toxicity, durability, and cost also influence the choice of materials for plasmonic applications. Gold, often used in combination with silver, remains a predominant choice due to its robust performance across both visible and NIR spectra. Other metals with plasma frequencies near UV wavelengths, such as cadmium (Cd), mercury (Hg), indium (In), lead (Pb), tin (Sn), and titanium (Ti), are not suitable for NIR sensing due to easy oxidation and high ohmic losses. Recent research has been directed towards exploring new materials that support plasmonic resonances at NIR wavelengths with lower losses. This search has included crystalline structured metals, intermetallic composites, metal alloys, nitrides, and oxides.

Other Geometries

Nanoparticles are capable of exhibiting highly localized plasmonic resonances when they are excited by light at specific wavelengths, causing their free electrons to oscillate. Coulomb forces balance out the tearing force that this oscillation generates. This section focuses on nanostructures that resonate at NIR wavelengths, with their spectral properties influenced by the nanoparticle's geometry and the coupling between particles. Recent advancements have led to the development of nanostructures with enhanced performance. These improvements are not only in their refractometric sensitivities but also in the ability to finely control their geometrical features. Such control is crucial as it allows for precise tuning of the plasmonic wavelengths through adjustments in size, aspect ratio, corner sharpness, heights, and even the spacing between particles. Additionally, there has been a push to increase the polarizability of each nanostructure by elongating and sharpening the particles. It is important to note that as the anisotropy of nanoparticles increases, the LSPR resonances evolve from simple dipolar modes to more complex multipolar resonances, which manifest as multiple resonant bands. When nanoparticles interact with each other, especially when they are arranged closely together or touching each other, their combined spectral properties change significantly through plasmonic coupling mechanisms. This coupling can substantially enhance the field around the nanoparticles as the interparticle spacing decreases. If nanoparticles are isolated, their geometry primarily determines how each field enhancement is produced. To give you an example, ellipsoidal nanorods show how changing a geometrical parameter, such as aspect ratio, can change their spectral properties by separating the dipolar mode into transversal and longitudinal modes that have different refractometric sensitivity and absorption intensities. In more complex nanostructures such as nanobars or nanoshells, even multipolar resonances can emerge. Recent trends have favored the creation of various polyhedral, disks, nanocrescents, and other intricate structures in pursuit of higher RI sensitivities and FOM. The structures that are long or have sharp tips work best because they create"hot spots" connected to multipolar resonances that have different refractometric sensitivity.

Moreover, collective interactions between nanoparticles play a critical role in altering the optical response of the entire assembly. Changing the distances between particles or the pattern in arrayed nanostructures is another way to tune the plasmonics, which is important for understanding how NP arrays and self-assembled structures behave in different wavelength ranges. Nanotriangles, nanorings, nanocrescents, and nanohole arrays made with nanosphere lithography

(NSL) can have different optical properties depending on the size of the nanospheres used to put them together. The interactions between nanoparticles depend a lot on how uneven they are. For example, nanotriangle arrays are more sensitive to RI than structures that are less uneven.

A nanostructure's shape factor, which is the ratio of a non-spherical nanoparticle's surface area to that of a perfectly spherical one, is also very important for making it more dipolar polarizable. For example, a nanorod with a higher aspect ratio is expected to achieve greater refractometric sensitivity improvements. This sensitivity is also wavelength-dependent, with higher sensitivities observed at longer wavelengths. Moreover, nanoparticles composed of different materials exhibit varying refractometric sensitivities due to their unique permittivities. This discussion underscores the impact of nanostructure geometry and material properties on the refractometric sensitivity, highlighting the complex interplay between nanoparticle design and optical performance.

Beyond Nanoparticles

Apart from simple nanoparticle-based LSPR sensors, there exists a category of sensors that utilize complex extended structures. These configurations take advantage of the geometry of planar nanostructures such as arrays of nanoparticles to produce plasmonic extinction spectra with high refractive index sensitivity and intense, narrow resonances. Henzie and colleagues, for example, employed sophisticated lithography methods to form multiscale nanohole arrays in gold films that display several plasmon resonances in the near-infrared portion of their transmission spectra [50]. These resonances achieve refractive index sensitivities up to 313 nm/RIU, with a narrowest of 14.5 nm. Another example is the regularly perforated metal film structures created by Liu et al. [51]. These structures have a sensitivity of 588 nm/RIU and an infrared region narrow reflectance peak (at 1.76 μm) due to competing bright and dark antenna modes. Interest has also grown in the LSPR sensing capabilities of nanostructures that display Fano resonances in their extinction spectra. Fano resonances occur in asymmetrical nanostructures (such as nonconcentric core-shell particles), where a typical "bright" plasmon mode that interacts with light interferes with a "dark" plasmon mode that does not. This interaction causes a big drop in the extinction spectrum, which should theoretically be very sensitive to changes in the refractive index. You can improve refractive index sensing even more by not only making the metallic nanostructures work better, but also by carefully planning the substrates that hold these structures in place. Dmitriev et al. showed big improvements in sensitivity by placing metal nanoparticles on dielectric pillars above the substrate [52]. This made it possible for solutions to interact more deeply with areas where the electric field intensity was higher. For nanodiscs, this approach doubled the sensitivity. While refining the shape, size, and composition of nanoparticles is beneficial, it represents only part of the solution to expanding LSPR applications in both science and technology. Other critical factors include the stability and availability of sensor substrates, their chemical interactions with analytes, and the capability for quantitative dynamic measurements.

Because there are so many different nanostructures out there, it is important to have a graph that shows how their LSPR wavelengths and RI sensitivities compare (Fig. 10). Nanorods are identified as promising candidates for these applications. However, the scarcity of data on the RI sensitivity of gold nanorods with aspect ratios exceeding 8 means they cannot be definitively ranked as the top choice. This lack of data does not stem from any physical or synthesis barriers that would limit their use in the desired wavelength range. Furthermore, nanorings are highlighted as viable nanostructural candidates, exhibiting some of the highest refractometric sensitivities.

Advancements in LSPR Modulation

Active control of LSPR using external stimuli like temperature, light, pH, electric field, and voltage is among the environmental stimuli that the metal plasmonic nanoparticles react to. The results of an experiment can be affected by the external stimuli's ability to deconstruct or assemble the nanoparticles. Generally, light is utilized as a stimulus to analyze the molecules' response using LSPRs. This stimulus can alter the assembly of the nanoparticles as well as the molecules being studied [53]. Controlling the assembly of plasmonic nanoparticles via external stimuli offers several advantages, including high accessibility to the states of the nanoparticle assembly and reversible control of the assembled states [54]. In this section, external stimuli are discussed looking at their impact on the LSPR. One of the stimuli is temperature, and when it rises, so does the rate of electron–phonon scattering, implying a rise in the plasmon oscillations' damping constant and dielectric permittivity, which broadens the LSPR band [55]. Lastly, the redshift of the LSPR is also influenced by the rise in the dielectric permittivity of nanoparticles with temperature, though the volume expansion of the nanoparticles is the primary cause of this shift [56]. Another stimulant that affects the array of nanoparticles is light. While bulk materials are only capable of exhibiting their intrinsic material properties, some nanostructured materials can be tuned for specific physicochemical qualities including light absorption, color change, and electrical and thermal capabilities [56]. The electron cloud is collectively energized as a plasmon when light interacts with free electrons. Plasmon and light inter-

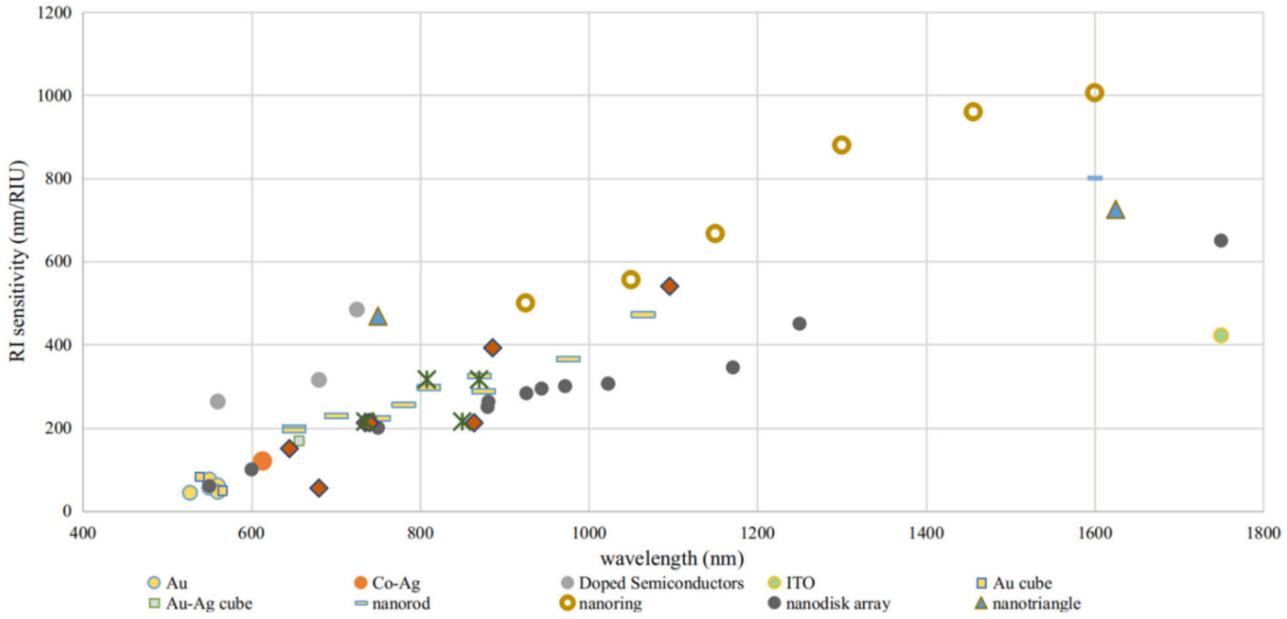

Fig. 10 This showcases a comparison of sensitivity versus wavelength for the most effective nanostructures in NIR sensing [41]

action makes it possible to localize light in subwavelength dimensions by breaking the diffraction limit of light. Strong electromagnetic (EM) field augmentation and improved optical near-field are produced by this localization of light in subwavelength dimensions. The array of nanoparticles is also influenced by pH, a qualitative measure of the sample (liquid) acidity or basicity. Research has shown that a variety of variables, including temperature and acidity, are significant determinants of nanoparticle size, shape, and color [57]. Using citrate as a reducing and stabilizing agent, Dong et al. (2009) demonstrated that the form of nanoparticles, specifically Ag nanoparticles, was greatly influenced by the pH. This indicates that the acidity of the solution has a considerable effect on the nanoparticles' shape [58, 59]. They discovered that at high pH, Ag nanoparticles were primarily spherical and rod-like in shape, whereas at low pH, they were primarily triangular and polygonal in shape Fig. 11 [59, 60]. Another stimulus that affects the nanoparticles' characteristics is an electric field, and when an electric field is applied and created by a fluctuating voltage, the sensing material's complex dielectric constant changes [61]. An electric field's application affects a material's optical characteristics. The LSPR shift changes as a result of an electric field's effect on the material interface's dielectric characteristics, as reported by M. Riswan et al. [62].

LSPR-Based Biological Sensors

Because it does not need labels, LSPR sensing has shown a lot of promise for biological and biomedical tests. ELISAs and other traditional assays use complicated exposure and rinsing steps with a secondary antibody to make a signal that can be detected. This signal indirectly shows that the target antigen is present. Label-free LSPR assays, on the other hand, directly detect a property of the target antigen molecule itself. This lets the concentration of the target on the sensor be tracked all the time and the binding process be studied in real time. The simplicity of label-free assays is evident as they require only a single capture antibody and less complex protocols compared to end-point assays. There is less need to use more analyte and less diffusion-limited mass transport when the sensing area is localized in nanoparticle-based LSPR assays. This makes the sensing process more effective. However, the absence of a signal amplification mechanism in label-free assays inherently limits their sensitivity. For instance, Figure 30 in [10] illustrates the saturation signal of an LSPR assay as a function of target concentration, following a 1:1 binding model where the detection signal peaks near the equilibrium constant inverse (K_{eq}^{-1}) of the capture agent. Although detection is possible below this concentration, the affinity of the capture agent fundamentally limits sensitivity. Numerous studies have demonstrated the application of LSPR sensing in biological assays and evaluated their performance. These studies are discussed in terms of the recognition interactions used, taking into account how various measurement aspects affect sensitivity and other performance metrics (Figs. 12 and 13).

The quantization and detection of viruses are utilized in various applications, such as food production, sanitation, environmental, clinical diagnostics, and food safety analysis [63]. Although they can have diverse mechanisms, most

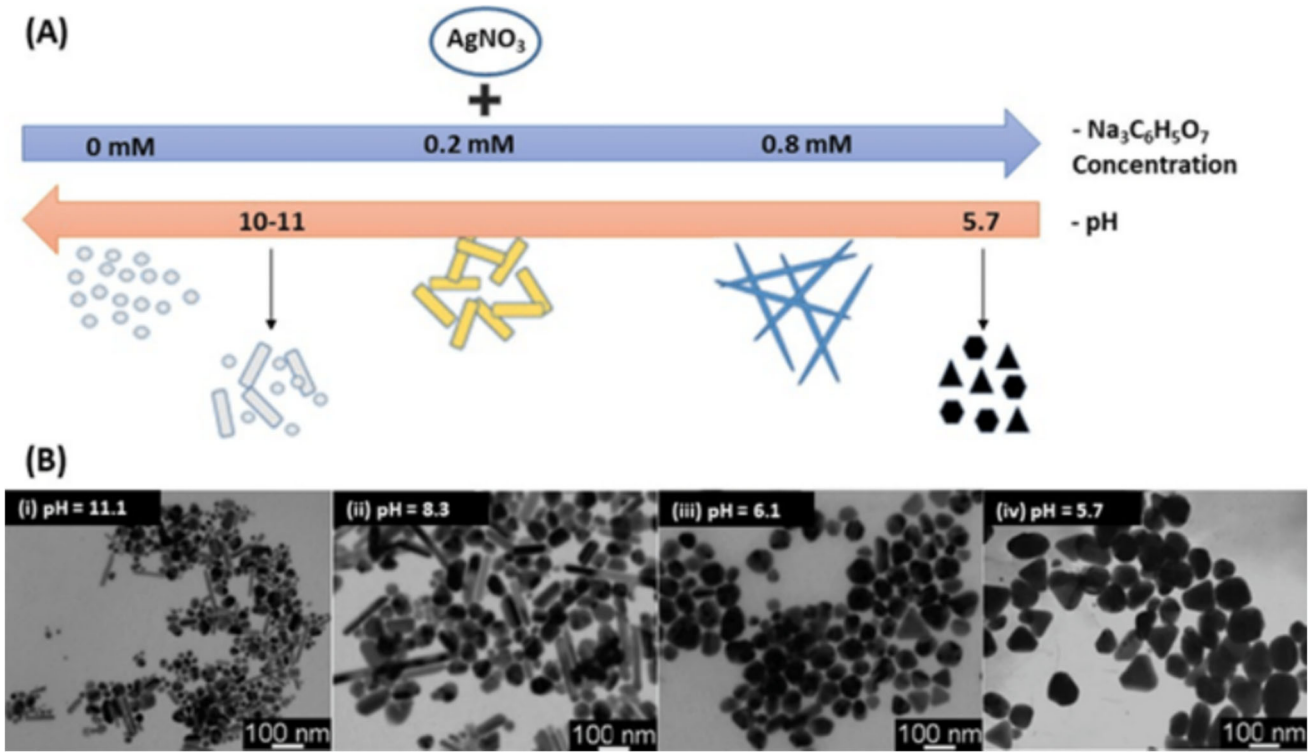

Fig. 11 The production of AgNanoparticles using citrate: **A** Experimental parameters influencing the morphology of the silver nanoparticles, or AgNanoparticles, and **B** TEM pictures of AgNanoparticles produced at various pH levels: I (11.1), II (8.3), III (6.1), IV (5.7). Taken from [59]

viruses comprise a combination of DNA or RNA genome and capsid proteins, which can be incorporated into an LSPR biosensor for detection. The majority of viruses that cause diseases are related to human pathogens. Usually, a disease is self-diagnosed by the host's immune response. However, most serious infections are unable to respond to the immune system's response and thus threaten the survival of the host [64]. One of the most common viruses that cause AIDS is HIV. The HIV-1 virus has a variety of generic symptoms, and as it is known today, it is a global threat [65]. To stand a chance in managing the development and spread of viruses such as HIV, rapid detection techniques development should be ceaseless. Due to the importance of virus detection in human health, rapid identification has gained widespread application. Unfortunately, current methods for quantifying and determining viruses are not sensitive enough.

Different strategies have been created to develop sensitive and selective LSPR-based sensors for the detection of viruses. The LSPR-based sensor produces a signal that is independent of the connection between the source and the channel, and the signal does not change the sample solutions' ionic strength in any way. Molecular interactions within

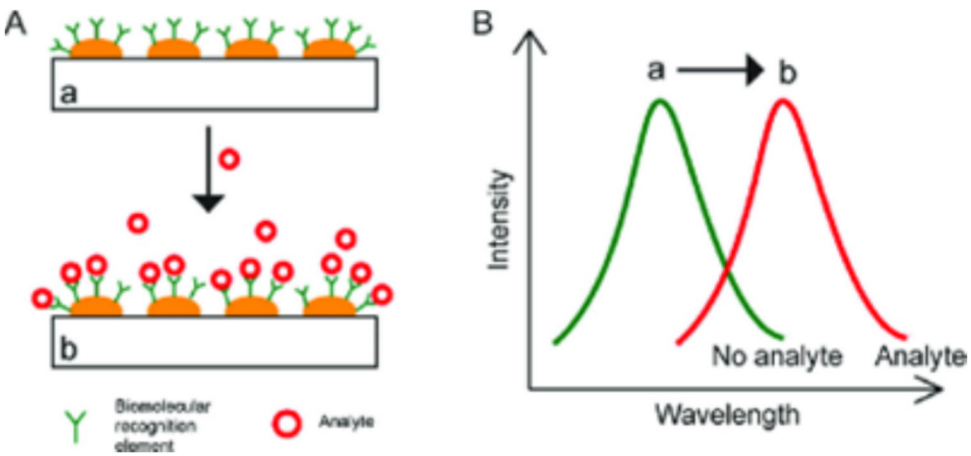

Fig. 12 Diagram representing the wavelength shift resulting from antibody-antigen binding events on the sensor surface (extracted from Zhou et al. [70]). The wavelength shift in the LSPR peak resulting from **a** (before analyte binding to recognition molecule) to **b** (after analyte binding to recognition molecule)

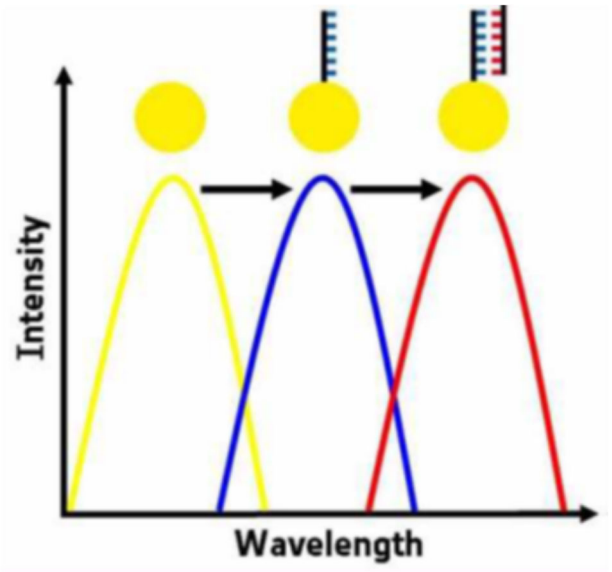

Fig. 13 Schematic diagram representing the wavelength shifts in LSPR peak on a single gold nanoparticle due to DNA hybridization between a target and a capture molecule. The yellow peak represents an LSPR peak resulting from gold nanoparticles. The blue peak represents an LSPR wavelength shift from the immobilization of a DNA capture molecule. The read peak represents a further LSPR wavelength shift resulting from the hybridization of a capture DNA molecule and a target DNA molecule

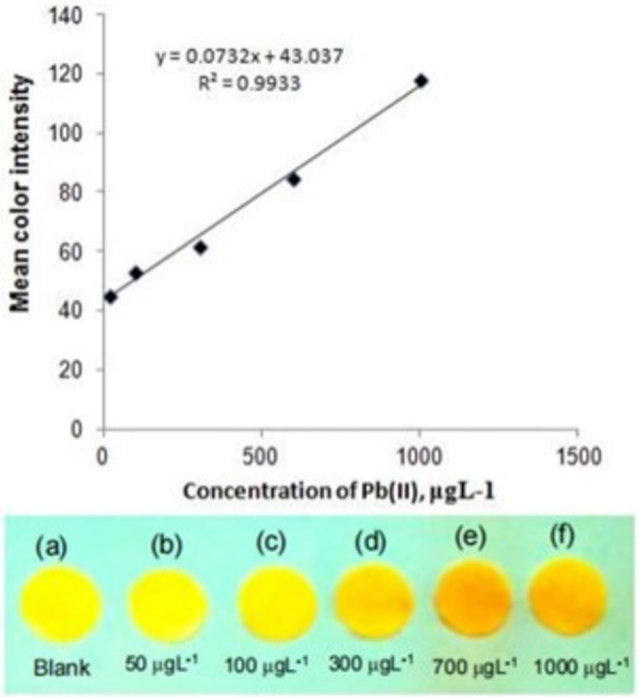

Fig. 14 Liner calibration curve indicating a relationship between the lead iron concentration and the resulting intensity, an experiment conducted by Shrivas et al. [74]

biological samples and receptors are essential. These interactions can be identified either by their physical or chemical properties [65]. Various biomolecules, such as antibodies, oligonucleotides, peptides, and enzymes, are immobilized on a substrate to detect an analyte or an organism of interest [66]. The detection and quantification of pathogenic viruses like HIV can be done at the protein level or nucleic acid level, depending on the point of analysis and different biomolecules or ligands can be employed for this detection [2]. The LSPR-based sensor can detect immobilized biomolecules and interactions with their specific analyte by converting the binding signals (physical or chemical) into electrical signals [67]. The binding events occurring at the surface of the sensor alter the surface plasmon, and this can be detected as a wavelength shit, as indicated below (Fig. 14) [68]. In protein recognition, the antibody-antigen interaction is the famous approach for LSPR-based sensor surface analyses. The well-documented high affinity between an antibody and an antigen makes it very easily detectable in LSPR biosensing, and it is displayed in LSPR wavelength shift as depicted in Fig. 14 [67]. A study by Inci et al utilized gold nanoparticles to accurately detect and quantify various HIV-1 subtypes (A, B, C, D, E, G, and other subtypes) from clinical blood samples. Absorbance changes were used to determine the presence of the HIV virus subtypes in the whole blood samples [69]. The changes in the refractive index of the gold nanoparticle surface from the label-free binding of specific monoclonal antibodies and the virus subtypes were detected as wavelength shifts in LSPR peaks.

When complementarity or reaction between the antibody and antigen of interest occurs on the sensor surface, a wavelength shift is produced from a change in refractive index on the sensor chip fabricated with nanoparticles. The quick and accurate identification of natural nucleic acids or disease-responsible nucleic acids, mostly DNA, is essential for different applications. The LSPR technique was utilized by Lee et al. (2006), to detect DNA-related interactions, by interpolating DNA between different nanoparticles both as a detection and nanoparticle coupling technique [71]. Further, Sönnichsen et al. [72], demonstrated successful DNA hybridization experiments through the use of double-stranded and single-molecule DNA molecules as molecular rulers between two nanoparticles for DNA detection. This was the first experiment in which a DNA hybridization step was performed on a single particle. This experiment achieved the LSPR sensing limit of 100 pM with an average density of only one DNA molecule per gold nanostructure [4]. A parallel approach with hundreds of nanoparticles could also show a limit of detection in femtomolar events. In addition to its well-known role as a carrier of genetic information, DNA possesses several unique characteristics. These include the ability for shorter DNA molecules to form self-assembly monolayers, self-complementary association into a double strand, and the potential to serve as a specific marker for

both genetic diseases and pathogenic microorganisms. These DNA biofunctionalized layers can stretch in a highly controlled way by binding the complementary strand, which, to some extent, enables the investigation of the effects of DNA surface concentration and surface distance. The study of this DNA-DNA interaction, or hybridization, is very desirable since it is a crucial mechanism in many areas of molecular biology and sensing [6]. LSPR-based sensors allow for the monitoring of DNA hybridization at the gold nanoparticle surface and a red wavelength LSPR peak shift due to binding is vividly observable in Fig. 14.

Figure 13 shows the DNA hybridization technique, which involves a capture oligonucleotide probe and a target single-stranded DNA strand that has been employed largely for different applications. The label-free detection of DNA hybridization has been applied as an alternative in new diagnostic procedures for diagnosing various illnesses and disorders involving DNA molecules. The obvious advantage of this procedure involves using a small amount of tissues or fluids. The capture probe used in this procedure can detect minute DNA sequences, which can represent the potential for future use in the detection of mutations [73].

Therapeutic and Imaging Applications: Plasmonic Imaging Techniques

Plasmonic imaging can be approached in two ways, far-field or near-field mapping [6]. One of the main goals of plasmonic imaging is to understand and maneuver nanostructures at the nanoscale for chemical sensing. Different methods can be developed to model and detect the different properties of metal structures accurately. Some of these techniques are based on conventional methods, such as UV–Vis-NIR spectroscopy, and dark-field microscopy [74]. Others utilize so-called sophisticated technologies to get incredibly detailed data. Today, it is possible to detect the presence of plasmons by using SERS, electron beams, or electric currents.

Far-Field Imaging

Analyzing individual nanostructures' properties is important for correlating LSPR and plasmonic strength. In the far-field imaging approach, the preparation of samples with low concentrations is required to ensure that the spacing between the particles is not too far away from the optical wavelength. This is done during the solution phase, though it is preferable to place them on a solid substrate. This allows for the correlation of the LSPR properties with the size and shape of the nanostructures. The optical resolution of Au nanoparticles allows the observation of the scattering patterns. In imaging, the brighter spots are the result of the enhanced aggregates' scattering, while the blueish spots are the result of single Au nanoparticles. Through the use of dark-field microscopy, we can collect the spectra of individual nanostructures [65]. This method can then be used to study their size, shape, and position. In addition, far-field imaging can monitor the changes in the spectrum of a single structure due to its different environmental conditions [68]. This method is very versatile and simple to analyze single nanostructures. Unfortunately, this technique is not ideal for smaller nanostructures, as absorption will dominate. The alternative technique, however, photothermal heterodyne imaging (PHI), was previously utilized to determine the nanoparticle orientation on a substrate. In this approach, the orientation of the nanorods is determined by using the SP oscillation's direction [1]. The orientation of a particle using far-field spectroscopy is very important for various applications, such as those that rely on the polarization of the excitation [75].

Near-Field Imaging

Unlike other optical spectroscopy techniques, near-field microscopy allows spatial resolution beyond the diffraction limit [5]. This makes it an ideal tool for analyzing plasmonic structures. Due to the small spatial oscillation of SP modes, subwavelength imaging is typically required to visualize their modes. In addition, the different SP modes' far-field properties can have identical properties, which makes it important to perform direct measurements of these structures [76]. A type of scanning probe known as near-field scanning microscopy (NSOM) uses a metal-coated probe to create an image by detecting evanescent signals. Its resolution is restricted mainly by the size of the aperture, and it can be used for measuring the distribution of nanostructures [3]. The acquired near-field images are developed using the detection of the scattered or transmitted light. They are characterized by the varying intensity of the light, which is determined by the position of the probe [4]. The images represent the electromagnetic states' density in the presence of the incident light. The most common type of imaging scheme for fluorescent substrates is the collection mode. In contrast, transmission mode is commonly used for detecting SP modes [3]. The aperture size is also affected by the transmission of power. Various apertures, such as crescent shape, have also been utilized to increase the power. A new generation of aperture-based systems is being developed. NSOM is based on an approach that closely resembles atomic force microscopy (AFM) which detects plasmons with high spatial resolution and allows for easy study of nanostructures [2]. In addition, AFM can be used to take images of topographic features. Scanning tunneling microscope tips can be used as probes for AFM and other types of optical systems. The radius of the tip's curvature determines spatial resolution, and the resolution of deep sub-wavelength areas can be achieved through infrared frequencies [3].

The ability to measure hundreds or thousands of nanostructures in parallel to increase sensitivity is made possible by advances in instrumentation and analysis. One such application is spectral image contrast-based flow digital nanoplasmon-metry (Flow DiNM), which was proposed to measure individual nanostructures [77]. The idea behind spectral image contrast is to compare the brightness of individual nanoparticles within two chosen wavelength ranges in their scattering picture. The area is represented by scattering brightness when the spectra are projected as scattering images [78]. Low throughput LSPR sensing is commonly carried out, with readout achieved by either individual, optically separated nanoparticles utilizing dark-field imaging or single spot readout from nanoparticle arrays [79, 80]. In an effort to enhance LSPR sensor throughput, nanoparticle arrays have been imaged without spectra being collected, which has reduced the amount of analytical data that must be collected. Using discrete LSPR sensors made of surface-confined nanoparticle arrays, the first demonstration of full spectral imaging of macroscale LSPR sensor arrays was shown to enhance throughput [81]. The enhancement is obtained by full access to either the visible or near-IR spectral spectrum provided by the white light that is used to illuminate the LSPR sensor arrays, liquid crystal tunable filter (LCTF) is used to specifically select the visible wavelength of light for transmission. A camera records a succession of pictures when the LCTF scans a wavelength, and those pictures are then examined to extract information about intensity [82].

Biotin-Streptavidin Interaction

The biotin-streptavidin interaction is frequently utilized in the development of biological assays due to its strong and specific binding affinity. This interaction is particularly advantageous for LSPR sensing because biotin, a small organic molecule, can be easily conjugated to the nanoparticle surface, facilitating the detection of the larger streptavidin protein through changes in the refractive index. Numerous studies utilizing LSPR assays have reported on biotin-streptavidin interactions, with sensitivities spanning from picomolar to micromolar concentrations. The wide range of reported performances is primarily attributed to variations in the equilibrium constant (K_{eq}) observed in dose-response curves. Although the affinity of biotin-streptavidin binding is typically very high—on the order of $10^{14}\,M^{-1}$, suggesting potential femtomolar sensitivities—the observed variations are often due to the effects of conjugating biotin to the nanoparticle surface. Factors such as steric hindrance and limited mobility due to the molecular tether can reduce the effective binding affinity. The specificity of these LSPR measurements is usually confirmed by the absence of a significant signal when exposed to non-specific targets such as bovine serum albumin, antibodies, or biotin-saturated streptavidin. Demonstrations of streptavidin detection in complex biological media like serum and dilute blood further underscore the robustness of this approach (see Figures 29 and 37 in [10]).

Antibody-Antigen Interaction

LSPR sensors have proven effective in immunoassay formats, where capture antibodies are typically conjugated to nanoparticle surfaces using Self-Assembled Monolayers (SAMs) and standard bioconjugate linkers. The sensitivity of these assays is generally evaluated through dose-response curves, depending on the binding constant and the signal-to-noise ratio. Unlike the biotin-streptavidin interactions, some immunoassays achieve equilibrium constants (K_{eq}) in line with their solution values, typically between $10^9\,M^{-1}$ and $10^{10}M^{-1}$. For example, Figure 30 in [10] illustrates a dose-response curve for detecting ADDL, an Alzheimer's disease marker, showing that antibodies can reach their natural affinity even when bound to nanoparticles. This is explained by the fact that they are comparatively bigger than biotin. The distance that this size creates between the nanoparticle and the target antigen increases and, however, may also lower sensitivity and the limit of detection. The picomolar range is often where sensitivity lies; however, there is not a set standard for determining the detection limit on different LSPR devices. Most reports on LSPR assays do not describe real-time interaction kinetics, which is a significant advantage of label-free assays. Instead, these assays are often used as endpoint assays, like those depicted in Figures 29 and 30 in [10]), which are valuable for comparative purposes. However, to fully leverage LSPR assays, monitoring and analyzing real-time binding kinetics is also feasible, especially for antigen-antibody interactions which occur at more practical rates compared to the extremely slow or diffusion-limited kinetics of biotin-streptavidin interactions. Figure 31 in [10] shows a kinetic analysis of antigen-antibody binding using a gold nanorod LSPR assay. Such real-time analysis allows for the observation of conjugation steps and multiple binding and unbinding events within a single experiment. This setup confirms binding specificity and interaction dynamics directly, offering a clearer insight than dose-response studies alone.

It's important to note that these kinetics measurements are most accurate when the binding is not diffusion-limited. If the target concentration is too low, diffusion effects dominate, and the observed kinetics will be slower than those of the first-order binding. This issue is exacerbated in very small sample volumes where diffusion limitations are significant. The mass transport of molecules in a flow cell is described

by the equation:

$$J = kC\frac{D^{2/3}}{u^{1/3}}$$

where J is the diffusion flux, k is a geometric constant of the flow cell, C is the analyte concentration, D is the diffusion coefficient, and u is the flow rate. High flow rates are necessary to overcome the low diffusion rates in SPR kinetics studies, where antibodies are immobilized within a polymer matrix rather than directly affixed to a surface.

LSPR-Based Sensing in Medicine

LSPR is mainly utilized in biosensing applications, such as detecting small molecules. Since bioreceptors and nanostructures have similar dimensions, they can be structurally compatible. This allows for miniaturization of signal transducers. The development of LSPR biosensors begins with the creation of biomolecule-biosensor conjugates, which are composed of nanostructures with unique electronic, catalytic, and optical properties. Functionalizing these materials with biomolecules can lead to the creation of novel substrates for various medical applications. The number of people with dementia is expected to increase significantly in developing countries. By 2050, it is estimated that over 70% of all individuals with this condition will be living in developing nations [2]. Developing a diagnostic test for Alzheimer's disease could help provide patients with more personalized treatment options. In a study conducted by Haes et al. [83], they proposed an LSPR-based biosensor that can monitor the interactions between an anti-amyloid β-derived diffusible ligands (ADDL) antibody and an amyloid-derived ligand. The use of Ag nanostructures with high selectivity for anti-ADDLs was demonstrated in their study [63]. The LSPR biosensor could be an economical and accurate method for performing clinical diagnostics.

In the study by Tessaro et al., the use of LSPR for ultrasensitive detection of the avian influenza virus using a gold surface was demonstrated [84]. The method was developed to allow the biosensing of the virus by binding a gold-binding polypeptide (GBP)-anti-influenza virus antibody protein to the gold nanoparticles. The GBP-fusion technique allows the attachment of bioactive molecules to gold surfaces without structural modifications [85]. This method could be utilized for the detection of various protein-protein interactions or clinical diseases. A method developed by Hammond et al. for the analysis of antigen-antibody correlations through LSPR-based sensing was shown to be easy, inexpensive, precise, and sensitive. It was demonstrated using antibodies such as IgG, IgA, IgG, IgD, and C-reactive [8]. Public health and economic losses are threatened by Salmonella. In developing nations, sporadic outbreaks are more common, but the combination of inadequate water quality and agricultural activities can increase the risk of foodborne Salmonella. The challenge of detecting bacterial pathogens remains high [65]. The LSPR-based method can be useful in detecting this pathogen, through capture probe and target pathogen DNA, the hybridization approach can be applied.

Other Biomolecular Interactions

LSPR sensing has been used to study various biomolecular interactions, including protein-carbohydrate interactions, aptamer-protein binding, cytochrome-inhibitor dynamics, nucleic acid hybridization, and toxin-receptor engagement, in addition to biotin-streptavidin and antibody-antigen interactions. Serum and whole blood are examples of complex media in which LSPR bioassays have also been performed. Yoo et al. measured label-free DNA hybridization using a multispot LSPR substrate, detecting mutations in the BIGH3 gene associated with corneal dystrophy [86]. They identified four gene variants with single-point mutations at a detection limit of 1 pM, demonstrating the assay's effectiveness even in patient samples containing both normal and mutant gene variants. In protein-carbohydrate studies, LSPR has been used to analyze the binding of concanavalin A (ConA) to sugars like mannose, which binds preferentially, showing not only high target specificity but also real-time kinetic monitoring. This approach has further extended to studying interactions involving cytochrome inhibitors and substrates, where significant shifts in LSPR peaks were observed corresponding to the binding events, demonstrating the method's sensitivity to small molecular interactions.

LSPR-Based Chemical Sensors

Gas Sensors

LSPR sensors have garnered interest for their rapid, label-free capabilities, extending beyond biological to chemical sensing applications. Cheng et al. [87] showcased LSPR sensing for volatile organic compounds (VOCs), such as toluene, using silver and gold nanoparticles and nanoshells. In their studies, they tracked how VOCs attached by looking at changes in the peak wavelength and the integrated extinction magnitude. These changes happened quickly and could be undone. The detection limit for toluene was established at 5 ppm. One of the latest improvements was a multiplexed sensor that used different self-assembled monolayers (SAMs) to make it more specific for different gases and reach detection limits as low as 16 ppm (see Figure 38 in [10]). Another LSPR-based gas sensing method was created by Karakouz et al. They used gold island films that were coated with polymers such as polystyrene sulfonic acid (PSS) and polystyrene (PS). These

films swell or shrink when exposed to gas, which changes the local refractive index and causes LSPR peak shifts (see Figure 39 in [10]). This method's detection limit was reported relative to the gas's vapor pressure at $0.05\,P_{sat}$.

Environmental Monitoring

The increasing number of people and the lack of natural resources have put a strain on the agricultural sector, and consequently on the economy. The LSPR-based sensing technique can help improve the efficiency of the agricultural industry by providing necessary information to farmers to use more effective and sustainable practices. Through the monitoring of plant nutrients, farmers can improve the quality and yield of crops. Currently, various methods are used to analyze plant nutrients, such as X-ray fluorescence spectrometry, inductively coupled-plasma emission spectroscopy, atomic absorption spectroscopy, and ICP-MS [76]. However, these instruments are laboratory-based due to their size, are labor intense, and require cooling, and gas supplies. LSPR technique however provides an alternative point-of-care testing, with enhanced detection limits and sensitivity for a laser-induced spectroscopy procedure for the detection of elements that are mostly plant nutrients like lead, potassium, calcium, iron, and copper. As compared to other detection methods, LSPR provides rapid and accurate analysis of these elements which is a critical part of farming. A detection device involving the paper-based lead ion analyzer was developed by Shrivas and colleagues. The device was modified with silver nanoparticles that are coated with polyvinyl alcohol. The LSPR red shift in the absorption band's frequency was caused by the interaction of the lead ions with the Ag NPs. The linear relationship between the calibration curve and the limit of detection displayed a good correlation with an R^2 value of 0.99 [74], as indicated in the figure below.

Surface water is believed to be the highest causative of environmental pollution because of the production of endocrine-disrupting chemicals (EDCs) such as dioxins, polychlorinated biphenyls (PBs), and agrochemicals [40]. These chemicals disrupt the development of the human body's endocrine system and also cause various other conditions, such as cancer. Thus, a rapid screening of EDCs is essential. Rindzevicius et al. [88] demonstrated the use of LSPR and SERS for measuring and detecting these substance substances. In their approach, they used a gold-capped nanopillar substrate, and the concentration of polychlorinated biphenyls in an area with high electromagnetic fields was achieved by forming clusters of micropillars. This concentration could then be further analyzed through SERS and LSPR techniques [89].

Also, a group of pesticides known as organophosphates are believed to pose a threat to human health, and thus are important targets for LSPR detection. The ability to detect these chemicals has been demonstrated through the covalent link between acetylcholinesterase (AChE) and nanostructures in a study conducted by Lin and colleagues. In their experiment, the different chemicals bind to AChE, and this interaction can be analyzed through SERS and eventually through LSPR [90]. A method for detecting mercury (Hg) by Rajeshwari et al has also been developed through LSPR-base sensing by monitoring the difference in the affinity between gold and silver nanostructures. The elevated levels of Hg in the solution caused changes in the gold nanostructures' aggregation state and thus shifts in LSPR peaks. This approach is important because, regardless of the metal's non-essential nature, living cells are prone to the toxicity of mercury [91].

An alternative approach in LSPR that can be exploited further to regulate LSPR sensitivity is the interparticle distance of nanoparticles in substrates [92]. The SERS enhancement then increases with decreasing gap distance between the nanoparticles. When two nanoparticles are positioned close to each other such that the gap is substantially less than the wavelength of light, near-field dipolar interactions take precedence [93]. As the separation is on the order of the wavelength, the far-field dipolar interactions become more prominent. Since a dipole field in one nanoparticle causes oscillations in another, the far-field interaction becomes a dynamic process [94]. To increase the LSPR sensitivity, the oscillation frequency can be modulated based on the nanoparticle distances between nanoparticles. This tunning can allow the LSPR to resonate at a particular frequency to increase the electric field for increased absorptivity of analytes. Thus, research has been carried out using the color change (absorptivity) in the solutions resulting from nanoparticle aggregation. Nanoparticle aggregation occurs when interparticle distance decreases and the resulting plasmonic coupling results in absorption spectrum shifts towards larger wavelengths [95]. This nanoparticle aggregation phenomenon is driven by different situations including biomolecular interactions (antigen-antibody) with nanoparticles and electrostatic interactions (pH changes). In biomolecular interactions, the nanoparticle surface is functionalized with the chemistry of different functional groups like thiols, amines, or polymer coating triggering nanoparticle aggregation [96]. This is important, particularly in biosensing where the detection of DNA/RNA and protein sequences in complementary DNA-functionalized nanoparticles leads to measurable signals. Through gold nanoparticle functionalization, for example, with specific antibodies for SARS-CoV-2 antigens, the

nanoparticles result in aggregate in the presence of the specific antigens which, in calorimetric tests results in color change, but in LSPR it results in wavelength shifts.

pH Sensors

LSPR sensors are also implemented in pH detection, often coupled with pH-sensitive polymers. Nuopponen et al. created a sensor with gold nanospheres covered in a pH-sensitive polymer. The sensor reacts to changes in pH between 5 and 8 by clumping together, but this process is limited by temperature and can not be undone. Later, Mack et al. unveiled a pH sensor based on plasmonic crystals that were composed of a responsive hydrogel-coated patterned polymer layer covered in a gold film. Over a pH range of 1.44 to 7.86 (see Figure 40 in [10]), this arrangement expands with rising pH, decreasing its density and producing blue shifts in the LSPR peaks (see Figure 40 in [10]). A pH sensor that uses gold nanocrescents on a substrate covered in a pH-sensitive hydrogel and works over a pH range of 4.5 to 6.4 was described by Jiang et al. It was found that the sensor was accurate to within 0.045 pH units, and the hydrogel-coated substrates were stable enough that the same results could be obtained after a month of storage (see Figure 41 in [10]).

Advancements in Renewable Energy Technologies

Understanding and optimizing the electrocatalytic and photocatalytic contributions of plasmonic nanoparticles are vital for their integration into renewable energy systems [97]. For instance, plasmonic nanoparticles can enhance the efficiency of photoelectrochemical water splitting, a key process in hydrogen production. By improving the rate and selectivity of reactions, plasmonic nanoparticles can make renewable energy technologies more viable and cost-effective, supporting the transition to sustainable energy sources. Recent studies have demonstrated the promising potential of using titanium dioxide (TiO) decorated with plasmonic metal nanoparticles, such as gold, silver, or copper, for visible-light-driven water splitting [98]. These nanohybrid systems can extend the light absorption of titania to the visible spectrum and facilitate the separation of photogenerated charge carriers, improving the overall photocatalytic efficiency compared to bare titania.

Other Chemical Sensing Applications

LSPR sensing has extended to detecting aqueous ammonia and copper ions. Dubas et al. [99] synthesized silver nanoparticles under UV light in the presence of poly(methacrylic acid), observing LSPR shifts upon ammonia exposure due to silver exchange with $Ag(NH_3)_2^+$ ions, altering particle size or shape [99]. Choi et al. created a copper ion sensor using gold nanoparticles that were coated with specific ligands [100]. When copper ions bind to the nanoparticles, they stop scattering, even at concentrations as low as 1 nM. He and his team used gold nanospheres that were modified with a chromophore to combine fluorometric and colorimetric sensing for copper ions. When copper ions are present, the chromophore decreases quenching and increases fluorescence intensity. This innovative use of plasmonic nanoparticles highlights their versatility beyond traditional LSPR applications.

Technological Advances in LSPR Sensing

Multiplexing

To compete with established assays like ELISA, LSPR sensing must be parallelized. To illustrate this, Endo et al. [101] deposited hundreds of antibody spots on a gold-capped nanosphere film, and at concentrations as low as 100 pg/mL, they measured optical absorbance to determine antibody affinity (see Figure 43 in [10]). In order to detect many targets without requiring spatial separation, Yu, Wang, et al. [102–104] devised a multiplexed LSPR sensing technique utilizing gold nanorods with varying aspect ratios (see Figure 44 in [10]). In an alternative approach using silver nanoparticles, Yonzon et al. [105] demonstrated duplex sensing with patterned nanotriangles modified for selective binding, allowing simultaneous monitoring of changes in the total extinction spectrum (see Figure 45 in [10]). Bingham et al. [106] introduced a method using a liquid crystal tunable filter in dark-field microscopy to image and analyze individual nanoparticles on a substrate, promising for future LSPR applications (see Figure 46 in [10]).

Integration with Microfluidics

LSPR sensors must be able to handle extremely small sample volumes with efficiency to be used in clinical settings [40, 107]. To overcome this, microfluidics is widely used, enabling high-throughput and high-speed sensing. An LSPR device connected with a single microfluidic channel that used just 1μL of sample volume was demonstrated in early work by Hiep et al. A layer of flat gold film covered in gold-capped nanospheres served as the substrate for the sensor (see Figure 47a in [10]). This configuration allowed for the measurement of insulin specific immunodetection as well as the bulk refractive index of glucose solutions, demonstrating real-time kinetics with a detection limit of 100 ng/mL. Subsequent developments by Huang et al. included a similar LSPR-microfluidic chip based on gold nanospheres, featuring an automated sampling system and dual microfluidic channels, handling 2.5 μL of sample volume. This setup

achieved refractive index measurement precision up to 10^{-4} RIU and demonstrated biotin/antibiotin binding (see Figure 47b in [10]). These chips utilized simple UV–vis absorbance spectrometers for signal detection. For scalability, innovative methods to read the optical extinction across multiple channels are essential. A scanning sample stage or a scanning detector based on a fiber optic probe could be one method. Another method might employ an LCTF-based LSPR imaging spectroscopy technique, identifying regions of interest on the substrate corresponding to different microwells for multiplexed measurements. Alternatively, as has been done in many LSPR sensing experiments, integrated intensity from several regions of a CCD image could be used in place of precise spectral data.

Optical Fiber Probes

Plasmonic nanoparticles integrated with optical fibers may provide remote, in vivo, and very small volume LSPR sensing. By adhering gold nanospheres to the fiber's end and monitoring the LSPR using the fiber's reflectance spectrum, Cheng et al. created a fiber-based LSPR sensor [108]. This setup was applied for bulk refractive index sensing, nickel ion detection, and biotin-streptavidin binding. Mitsui et al. [109] refined this approach by using the total reflection intensity of a red LED instead of a white light source and spectrometer, demonstrating time-dependent measurements of biotin-streptavidin binding with a precision of 2×10^{-5} RIU. Further innovations by Tang et al. involved a long-period fiber grating (LPFG) LSPR sensor where a segment of the optical cladding was removed, and gold nanospheres were deposited directly on the fiber [110]. This modification allowed coupling of the LSPR-associated evanescent mode of the particles with the fiber's optical modes, creating a refractive-index sensitive dip in the fiber transmission at IR wavelengths. This device showed high sensitivity for dinitrophenyl (DNP)/anti-DNP sensing with a detection limit of 0.95 nM (see Figure 48 in [10]). Shao et al. also talked about a sensor that used a polyelectrolyte layer to help gold nanospheres stick to an unclad part of an optical fiber [111]. We did LSPR sensing by checking the total fiber transmission and got a sensitivity of up to 13 AU/RIU for changes in the bulk refractive index. Specific antibody sensing was demonstrated, although improvements in target detection might be achieved by reducing the capture layer thickness (see Figure 49 in [10]).

These advancements are steering LSPR towards becoming a feasible sensor technology for both laboratory and clinical applications. Future sections will discuss further developments and requirements to transition LSPR into a practical technology.

Localized Surface Plasmon Resonance Imaging and Application of Machine Learning

Label-free optical imaging of nanoscale items encounters inherent difficulties. Methods utilizing propagating SPR and LSPR have demonstrated potential. Nonetheless, achieving diffraction-limited resolution and improved surface localization in SPR imaging continues to present significant challenges. Localized Surface Plasmon Resonance imaging (LSPRi) is a powerful optical biosensing method that uses the way that light excites the conduction electrons on the surface of metallic nanoparticles to make them oscillate. LSPR is a good way to find molecular interactions in real time without labels because the resonance is very sensitive to changes in the local dielectric environment.

LSPR happens when light hits metal nanoparticles, usually gold or silver, and causes their conduction band electrons to collectively oscillate on the surface of the nanoparticles. The frequency of these oscillations depends on the particle's size, shape, and the dielectric properties of the surrounding medium. When the frequency of the oscillations matches the incident light's frequency, maximum absorption and scattering occur, leading to a pronounced peak in the extinction spectrum. This peak is highly sensitive to changes in the local environment, such as the adsorption of biomolecules onto the nanoparticle's surface.

LSPR Imaging Techniques

In LSPR imaging, changes in the optical properties of nanoparticles are monitored to detect molecular interactions at the sensor surface. Many times, techniques like dark-field microscopy, scanning electron microscopy, and surface plasmon resonance microscopy are used to improve the imaging, which lets scientists see the interactions at the nanoscale level more clearly. This makes LSPR imaging particularly useful in medical diagnostics, environmental monitoring, and food safety testing.

Nanoparticle Coupling for Enhanced LSPR Sensing

The fundamental nature of light-matter interactions on nanoparticle arrays makes LSPR an ideal platform for scientific discovery. The nanoparticle's structural changes, typically caused by aging and surface energy minimization, have been utilized to create a new class of colorimetric for time and temperature indicators [66]. The effect of struc-

tural changes is documented in a study by Kelly et al in Ag nanoparticles, and if the sharp corners of Ag nanoplates are modified to a shorter size and spherical shape in solutions, it results in a significant shift in their LSPR [112]. This study reports that the Ag nanoplates' rounded corners are sensitive to temperature, and higher temperatures are used to modify and round the nanoplates [8]. These changes can be colorimetric and LSPR shifts analyzed. The nanoparticle structural changes application has resulted in further developments in LSPR detection and sensing, with the main focus on enhancing the sensitivity of nanostructures. Through coupling a molecule to a nanostructure's resonance frequency, the LSPR's peak shift is significantly increased [113]. An increase in the peak LSPR shift occurs when there is an overlap between the molecular electronic and LSPR spectra. The electronic structure of an adsorbate is sensitive to this coupling phenomenon, which then consequently generates a large spectral shift. The LSPR coupling technique allows for the detection of low-saturation polymers by monitoring a small number of molecules [65]. Through the interaction between the molecules and the nanostructures, the electronic structure of a given molecule changes and this leads to a detectable plasmonic change. In an experiment by Querebillo [114], the heme-based cytochrome P450 protein, which is adsorbed on Ag nanostructures, had an altered electronic structure due to the camphor binding. The observed LSPR shift, which was 67 nm, was linked to a 0.07 nm shift per camphor, and this can thus be further used to make the instrument sensitive to single molecules [114, 115]. However, the nanostructure approach through the interaction of biomolecules needs to be studied further to optimize the coupling technique. Another alternative coupling approach to enhancing LSPR sensitivity is the incorporation of distance-dependent [71]. When nanostructures are coupled with each other, a fundamental SP mode emerges, which is generally redshifted relative to the structures located on the other side of the gap. The shift's sensitivity to the gap's width is usually 10 nm. This approach can be further applied by the addition of ligands or proteins that will bind to the nanoparticles, and the interactions between them can then be analyzed by the gap-dependent LSPR shifts [116, 117]. This approach usually requires low molecule amounts in the gap region, and these shifts can be observed with the naked eye or by a simple microscope. The use of distance-dependent coupling for LSPR sensing largely involves forming aggregates through the DNA molecule [118]. Some of the most advanced studies have utilized the gap width dependence technique to analyze the dynamic changes in the arrangement of nanoparticles and their associated molecules. This method can be used for long-term molecule interaction monitoring and nanoparticle distance between a few nanometres and up to 70 nm can be achieved.

Maximizing the Molecular Detection Sensitivity of LSPR

Molecular Detection with Single Nanoparticles

As was previously mentioned, LSPR measures alterations in the dielectric environment brought about by molecular binding, which enables it to detect molecular interactions close to the nanoparticle surface. In particular, elongated-shaped gold and silver nanoparticles provide high refractive index sensitivities that are localized to the nanometer-scale volumes surrounding their sharp points. The expected result is a discernible shift in the plasmon resonance peak wavelength if a macromolecule, like a protein, enters this compartment that has a refractive index different from the surrounding medium. Historical data show that LSPR molecular sensing has progressed to the detection of single molecules. The plasmon resonance shift seen by Haes et al. was caused by the nonspecific attachment of about 700 streptavidin molecules to a single silver nanoparticle [83]. Similarly, McFarland and Van Duyne measured shifts caused by roughly 60,000 hexadecanethiol SAM molecules on silver nanoparticles [119]. Later research by Rindzevicius et al. and others has focused on gold-based sensors [88]. Biotin was used as a recognition agent for streptavidin detection, which made the sensors even better at finding small molecules [88].

Nusz et al. enhanced these methodologies on single gold nanorods, achieving detection limits down to 1 nM for streptavidin, corresponding to about 18 molecules per nanorod [10]. These studies underline the potential for single-molecule detection through careful optimization of nanoparticle geometry and the experimental setup. At the same time, Unger et al. did work using dielectric colloids attached to gold nanocrescents that supported the idea of single-molecule LSPR sensing even more. This showed that even small binding events might be able to be detected with better particle design and illumination intensity. Later, by seeing distinct blue shifts in the LSPR peaks that corresponded to the rate at which antibody-antigen couples split apart on a gold bipyramid, Mayer et al. were able to identify a single molecule. Currently, the primary task is to increase the signal-to-noise ratio in LSPR peak wavelength shift measurements in order to improve the systems' ability to detect molecules. Recent advances by researchers like Käll and Chen have demonstrated sensors with extremely fine resolution, allowing for the detection of low concentrations of analytes such as prostate-specific antigen.

LSPR as a Single-Molecule Method

Single-molecule sensing via LSPR benefits from its non-invasive nature. There is no need to chemically alter the

target or bind other components in order to produce a signal because the measurement directly measures the refractive index of the target molecule optically. LSPR measurements do not include any applied stress or tension, which can alter binding strengths, in contrast to force-based sensing techniques. The target molecule in these studies is exclusively affected by the optical near-field of the nearby nanoparticle. In the past, whispering gallery mode microtoroid resonators were used for label-free optical detection of single molecules. These devices have high signal-to-noise ratios because they have high-quality factors. However, LSPR sensors provide advantages in simplicity and do not require complex microfabrication, making them suitable for applications in proteomics, diagnostics, and drug discovery. The ability of LSPR to monitor interactions over extended periods could make it a valuable tool in the arsenal of single-molecule detection techniques.

The Role of Metal Nanostructures Dimmers and Trimmers to Molecular Detection

The LSPR nanostructure dimers and trimers are used in molecular detection and sensing applications due to their high sensitivity to changes in the local refractive index [120]. This property can be exploited to detect the adsorption of thin films on the nanostructure surface, with the resonance frequency shifting as the film thickness increases. For example, gold nanocages have found widespread use in theragnostic applications, where they can serve as substrates for the detection of trace biomarkers using spectroscopic methods, function as contrast agents for optical imaging, act as carriers for drug delivery, and serve as transducers for photothermal therapy. The proximity influence of target molecules can be considered as a slight increase in the local refractive index against the original index in either the air or water, which can significantly modulate the resonance frequency of the LSPR nanostructures [121, 122]. Nanomaterials such as carbon quantum dots have also been employed to modify SPR sensors to overcome the limitations of low sensitivity for detecting normal or extremely low levels of analytes like dopamine. The ability to precisely control the design of plasmonic-based sensors through theoretical analysis is crucial for optimizing their performance in various applications.

Future Directions

The field of LSPR is continuously advancing, with research aimed at creating sophisticated nanostructures, discovering new materials, and broadening the scope of applications. Future research directions include integrating LSPR with other nanomaterials, such as 2D materials and quantum dots, to form hybrid systems with improved functionalities. One significant challenge is developing large-scale, cost-effective fabrication techniques for LSPR nanostructures to enable widespread practical use. Additionally, a fundamental understanding of LSPR mechanisms, especially in complex nanostructures and coupled systems, remains an active research area. Researchers are developing advanced computational methods and in situ characterization techniques to gain deeper insights into LSPR phenomena and guide the rational design of LSPR-based devices.

Integration with Machine Learning

It is possible to improve the sensitivity and selectivity of LSPR imaging with machine learning (ML) [123–126], which lets you do complex data analysis and pattern recognition that is hard to do with traditional methods. Machine learning algorithms can analyze LSPR data to distinguish between noise and actual signal changes resulting from molecular interactions. Techniques like principal component analysis (PCA) and support vector machines (SVM) can in principle classify and predict changes in the LSPR signal due to different analytes and for application diagnostics. ML can be used to build models that predict the outcome of complex biochemical interactions based on historical LSPR imaging data. Neural networks, for instance, can learn the characteristics of specific binding events, enabling the prediction of binding affinities and kinetics. By applying algorithms such as genetic algorithms (GAs) or deep learning, researchers can optimize the design of nanoparticles for specific applications. These machine learning models can simulate and guess how changes in nanoparticles' shape, size, and material will affect their LSPR properties. This can help with making nanoparticles with the properties that are wanted. Machine learning models can also be integrated into LSPR imaging systems to provide real-time feedback and control. This application is crucial in dynamic environments where conditions change rapidly, such as in live cellular assays or during complex chemical reactions. In the field of medical diagnostics, ML-enhanced LSPR imaging can be used to detect and diagnose diseases by recognizing patterns associated with specific biomarkers. This application has the potential to provide rapid, accurate diagnostics with minimal sample processing, making it invaluable in settings lacking extensive laboratory facilities. While the integration of machine learning with LSPR imaging holds significant promise, challenges remain, such as the need for large, annotated datasets to train the algorithms, and the complexity of integrating ML algorithms into real-time, high-throughput LSPR systems. Future research will likely focus on developing more sophisticated algorithms that can operate efficiently with smaller datasets and integrating these systems seamlessly with existing optical and nanofabrication technologies.

Integration with Quantum Technologies

Quantum technologies are finding their way into plasmonics based biosensing [127–135]. Some research is currently being conducted specifically in the integration of quantum technologies with LSPR. Ugwuoke et al [136] wrote an article which gives a theoretical model for a nanosensor system that uses quantum plasmonics to improve sensing of the refractive index by using photon correlations. The authors in their paper modelled a system that uses a quantum emitter (QD) and a metal nanoparticle (MNP) to improve sensing performance by taking advantage of higher-order photon correlations. The paper concludes that while the proposed quantum LSPR-based plasmonic sensor shows promise for enhanced refractive-index sensing, practical implementation requires overcoming challenges such as low mean photocounts and optimizing system parameters for significant noise reduction. This type of work highlights the potential of integrating quantum technologies with LSPR.

Extraordinary Optical Transmission

Extraordinary optical transmission (EOT) refers to the phenomenon where light passes through subwavelength apertures in a metal film with an efficiency much higher than predicted by classical aperture theory [138]. Discovered in 1998, this remarkable property of EOT has been attributed to the excitation of surface plasmons, which are collective oscillations of free electrons at the metal-dielectric interface. The coupling of incident light with these plasmons leads to enhanced transmission through the nanoholes or slits, despite their subwavelength size (see Fig. 15). EOT has spurred extensive research due to its potential applications in various fields, including sensing, imaging, and photonic devices. The ability to control and manipulate light at the nanoscale opens up possibilities for developing highly sensitive sensors, efficient photonic circuits, and novel optical devices.

The primary mechanism behind EOT involves the interaction of light with surface plasmons on the metal film's surface. When light strikes the periodic nanostructures, it excites surface plasmon polaritons (SPPs), which propagate along the metal-dielectric interface. These SPPs can tunnel through the subwavelength apertures, re-emerging on the other side and enhancing the transmitted light intensity. Additionally, localized surface plasmons (LSPs) excited at the edges of the apertures contribute to the enhanced transmission. The efficiency of EOT can be significantly influenced by the design and fabrication of the nanostructures. Factors such as the shape, size, and arrangement of the apertures play crucial roles in determining the optical response. Recent studies have explored various configurations, including circular, elliptical, and rectangular holes, as well as slits and hybrid structures combining nanoholes with nanoparticles or nanodisks.

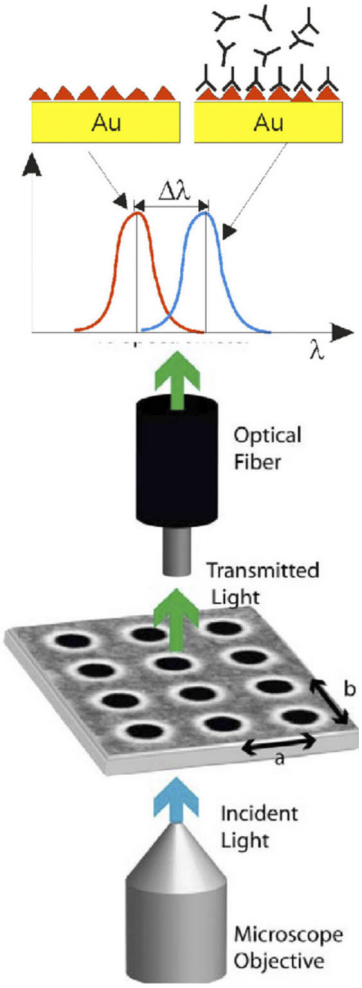

Fig. 15 The remarkable optical transmission-based biosensing concept. A biological target-coated gold (Au) film has a series of nanoholes drilled in it to transmit white light from a microscope. An optical fiber receives the transmitted light, analyzes it, and produces a spectrum with a peak at a specific wavelength (λ). When a solution binds to an immobilized target, the transmitted spectrum shifts, causing a peak shift (Δλ) [137]

Advanced fabrication techniques, such as electron-beam lithography, focused ion beam milling, and nanoimprint lithography, have enabled the precise creation of these nanostructures. These methods allow for the fine-tuning of the geometrical parameters to optimize the coupling and resonance conditions of the plasmons, thereby enhancing the EOT effect. The choice of materials for EOT structures is another critical aspect. While noble metals like gold and silver are commonly used due to their excellent plasmonic properties, recent research has explored alternative materials such as aluminum, copper, and even graphene. These materials offer different plasmonic characteristics, enabling the tuning of EOT across various spectral regions, from visible to infrared. Moreover, the incorporation of dielectric materials within the apertures or as surrounding layers has been shown to modulate the plasmonic response. For example,

loading nanoholes with dielectric substances can shift the resonance wavelength and improve the sensing capabilities of EOT devices.

EOT has proven to be highly effective for sensing applications, particularly in detecting biological and chemical substances. The sensitivity of EOT-based sensors arises from the strong interaction of plasmons with the surrounding medium. Changes in the refractive index or the presence of specific analytes near the nanostructures lead to measurable shifts in the transmission spectrum. Recent advancements have demonstrated the use of EOT for real-time, label-free biosensing with high sensitivity and specificity. The integration of EOT structures with microfluidic systems and optical fibers further enhances their applicability in practical sensing platforms. In the realm of photonics, EOT structures are being explored for their potential in creating compact, efficient optical components. These include filters, modulators, and waveguides that leverage the enhanced transmission and field confinement properties of EOT.

Localized Surface Plasmon Resonance Sensor as a Laboratory Instrument for Molecular Biology

Given the current technological landscape as discussed in previous sections, LSPR sensors are poised to rival commercial SPR instruments with some key improvements. The simplicity and lower cost of LSPR, sometimes described as "SPR in a cuvette," suggest significant potential, but several challenges remain. Sensitivity is the foremost; while single-particle, single-molecule measurements offer maximum sensitivity and valuable insights into molecular dynamics, they are impractical for broader SPR-like applications. Rather, the emphasis should be on improving the sensitivity of stable substrates that are based on nanoparticle ensembles. Significant progress has been made, as evidenced by the development of very sensitive gold nanodisc ensembles that can detect PSA at 30 pM. Additionally, achieving greater robustness and consistency across LSPR substrates is crucial for ensuring reproducible and reliable measurements. LSPR sensors must be able to identify analytes in complicated biological samples such as blood, serum, or urine in both real-world and some laboratory environments. In terms of specificity and optical design, this can be challenging. For these applications, the use of glass substrates in a reflection geometry may be especially beneficial. The inexpensive nature of LSPR sensors is a big advantage. A basic home-built LSPR system utilizing white-light extinction can be assembled for under $25,000, with potential for further reductions as the technology and instrumentation evolve. Innovations such as using simple LED-based light sources and photodetectors, as well as integrating fiber optics and microfluidics, could further reduce costs and enhance the functionality of LSPR sensors, making them more versatile and efficient for benchtop use.

LSPR Sensing as a Medical Diagnostic Tool

The simplicity, speed, and cost-effectiveness of LSPR sensing make it a promising candidate for medical diagnostic applications, particularly for point-of-care settings. The development of robust, portable LSPR devices could revolutionize diagnostics, especially in resource-limited settings. Neuzil and Reboud have pioneered a hand-held LSPR device that replaces traditional white-light and spectrometer setups with four distinctively emitted LEDs and a simple photodiode for reflectance measurement, significantly reducing the cost and complexity of the device. This innovation demonstrates the potential of LSPR sensing for practical medical diagnostics. Moreover, companies are already exploring commercial LSPR-based medical devices. Anti-streptavidin has been found in buffer solutions and urine as part of demonstrations. This shows that the technology can be used on real biological samples with limits of detection in the nanomolar range. Future development of LSPR-based medical diagnostics will need to address several challenges, including enhancing molecular detection sensitivity, enabling effective operation in complex fluids, further device miniaturization, and creating user-friendly interfaces. These advancements will help tailor LSPR technology for widespread clinical use, where it could significantly impact proteomics, diagnostics, and drug discovery.

Metamaterials for LSPR

Metamaterials are artificially engineered structures designed to control and manipulate physical properties of waves, such as electromagnetic, acoustic, or thermal waves, in ways that natural materials cannot [139]. These materials derive their unique properties not from their chemical composition but from their carefully designed structures, often at scales smaller than the wavelengths of the waves they influence. Metamaterials, which are artificially structured materials with unique properties not found in nature, have been extensively explored to enhance and control LSPR properties. Metamaterials that support LSPR offer exciting opportunities for enhancing light-matter interactions. By carefully designing the composition and structure of these materials, it is possible to achieve significant improvements in optical sensing, energy harvesting, and nonlinear optics.

Dynamic Tunning of LSPR for Advanced Applications

Noble metal nanoparticles are employed extensively as optical labels and chemical sensors because they do not photobleach and have substantial absorption and scattering

coefficients at wavelengths that may be controlled by varying the particle size, shape, and refractive index of the surrounding medium [140]. By precisely controlling nanoparticle characteristics, size, and dielectric surrounds, optically resonant nanostructures serve as optical antennas and allow for the deterministic construction of optical properties [141]. The ability to control the optical response actively and dynamically, particularly the optical resonant wavelengths of nanostructured elements, would enable a wide range of applications [142]. In addition to being often used to control the bulk optical absorbance of thin films, electrochromism is also occasionally employed to regulate the optical characteristics of subwavelength resonant nanostructures. These kinds of demonstrations typically alter the dielectric 2 media's optical characteristics around metallic subwavelength nanostructures. Although promising, current demonstrations use liquid electrolytes, which restricts their use for resonant optical coatings and devices on-chip [143]. Many studies in this area also use polymer electrochromic because they switch quickly in the millisecond range, and have low thermal sensitivity [70].

Molecularly Imprinted Polymer (MIP)-Based LSPR Sensors

A molecularly imprinted polymer (MIP) is a nanostructured polymeric material obtained through molecular imprinting, which involves the formation of a pre-complex of a structured template (molecules, atoms, etc.) and specific functional monomers. The next step involves polymerization and cross-linking of the pre-complex to form a polymer with a trapped and fixed template. After the removal of the template molecules, the resulting structure with empty selective binding cavities is hence termed the molecularly imprinted polymer [122]. The appearance of a certain polymer chain nanostructure can be attributed to the fixation of the template molecules during the process of polymer synthesis. In MIP synthesis, molecular recognition between molecules (DNA or proteins) and synthetic materials is vital for a "memory" polymer. The matrix structure of the molecules that were used as templates can be recalled, as rebound targets, through molecular imprinting, and thus MIP has an increased selectivity [144]. This concept is instrumental in the development of new materials that can be used for applications in sensor materials. One of the first studies involving the synthesis of MIP by silica matrices was reported by Polyakov in the 1930s. Since this groundbreaking study, the popularity of MIP has increased significantly [145]. In the succeeding studies conducted in the 1950s and 1970s, researchers noted that using alkylbenzenes for synthesizing silica polymer exhibited a significant increase in its selectivity when it came to adsorbing hydrocarbons [146]. In addition to these findings, they also noted that the introduction of the template during the polymer synthesis process affected the silica's adsorptive and pore size characteristics [147]. Therefore, the synthesis approach should be well-optimized for a specific design and application. Due to their selectivity, stability, and high affinity in target recognition, the MIP approach has gained considerable interest in its application in sensors [148]. Their ability to selectively capture a target molecule in complex media generally does not involve the sample pre- and post-treatment making them ideal for diagnostics in point-of-care settings. These characteristics make the MIP appealing for incorporation and modification with the LSPR-based sensors, especially in efforts to develop point-of-care technology. In SPR sensing, the MIP layer is utilized as a recognition layer which serves as memory-imprinted sites of the templates for the detection [149]. When the template molecules come into contact with the recognition sites, the binding is non-covalent, and this binding results in a change in the refractive index. This refractive index change can then be observed by the shift in the resonance wavelength. As already discussed, when metal nanoparticles are introduced instead of a metal thin film, the phenomenon known as LSPR will occur. This is more sensitive than in SPR studies when it comes to biomolecular interactions. Although the refractive index sensitivity of SPR is higher than that of LSPR, the LSPR's sensitivity is higher when it comes to biomolecular interactions. This is because the electric field is confined within a small sensing volume. In LSPR-sensing therefore, the MIP layer is typically coated with metal nanoparticles to act as the sensing medium and increase the sensitivity for biomolecular interactions.

Comparison of the Localized Surface Plasmon Resonance to Alternative Label-Free Techniques

Label-free sensors detect target molecules directly through their inherent properties, such as changes in the refractive index. Localized surface plasmon resonance fits well into this category as it directly measures these changes without the need for labels. This contrasts sharply with most biological sensors that rely on labels like radioisotopes, fluorophores, or enzymes to amplify signals. For example, in enzyme-linked immunosorbent assays (ELISA), an enzyme activates a dye molecule upon binding to the target, allowing detection of minimal sample quantities due to signal amplification (see Figure 14 in [10]). While labels enhance signal detection, they can also interfere with natural biomolecular interactions, making label-free techniques preferable for studying biomolecules in their native states.

Label-based assays typically require multiple antibodies and provide only endpoint measurements, whereas label-free methods like LSPR offer real-time kinetic data and gener-

ally need only a single antibody. Surface plasmon resonance is another label-free technique, utilizing changes in refractive index sensitivity measured by the reflection of laser light through a prism off a gold film. Although SPR can detect sub-monolayer analyte quantities and provide kinetic data, its lack of a localized sensing volume often necessitates a thick polymer layer suffused with a capture antibody for effective signal generation.

SPR is extensively used in biomolecular interaction studies and antibody screening but is less common in clinical settings since it is less sensitive than techniques such as ELISA, complex optical setups, and precise temperature control requirements. In contrast, LSPR, with its simple optical extinction measurement technique, is not temperature-sensitive and requires only basic laboratory equipment. LSPR's highly localized sensing volume also obviates the need for a polymer matrix to trap interacting molecules, often necessary in SPR measurements (see Figure 16 in [10]).

Yonzon et al. [105] conducted a side-by-side experimental comparison of SPR and LSPR by observing the binding of concanavalin A (ConA) to monosaccharides on silver nanoparticles. Although the unbinding signal was smaller in LSPR, due to its smaller sensing volume, the signal-to-noise ratio was significantly higher in SPR. Later, Svedendahl et al. compared these techniques under identical conditions for biotin-streptavidin binding [150]. They noted similar molecular sensing performance, attributing it to the long decay length of propagating plasmons compared to localized nanoparticle plasmon modes. Despite similar sensitivity, the effective detectivity was higher in LSPR due to the reduced gold surface area involved (see Figure 17 in [10]).

Beyond optical methods like SPR, label-free biosensing can also be realized through mechanical force transduction. An illustrative example involves the measurement of deflections in an atomic force microscopy (AFM)-like cantilever, which has been functionalized on its surface. This deflection results from changes in mass and surface tension when a target molecule binds to the surface. These mechanical sensors can detect single-molecule binding events but often require complicated transducer fabrication and precise measurement setups, limiting their broad applicability. Ndieyira et al. utilized this method to explore antibiotic resistance mechanisms in bacteria by assessing the binding affinity of vancomycin, an antibiotic, to mucopeptides located on bacterial cell walls. This was conducted in a multiplexed setup where various cantilevers were modified with different ligands, detecting vancomycin concentrations as low as 10 nM (see Figure 19 in [10]). Ultimately, the choice of label-free technique depends on the specific application, sample complexity, required sensitivity, and available resources.

Additionally, label-free sensing has been successfully implemented in semiconductor nanowire systems, where changes in conductance across a nanowire are measured following the binding of charged biomolecules. Chua et al. applied this technique for the ultrasensitive detection of cardiac troponin-T (cTnT), a critical biomarker for myocardial infarction. In their experiment, silicon nanowires were functionalized with antibodies specific to human cTnT, achieving detection thresholds as minute as 1 fg/mL, or 3 attomolar (see Figure 20 in [10]).

Ahl, Yu, et al. introduced a novel nanoporous gold substrate supporting both SPR and LSPR modes, fabricated via a chemical dealloying method [151]. They demonstrated that while LSPR sensitivity decays with distance from the surface, SPR sensitivity remains constant up to 18 dendrimer layers, emphasizing the unique characteristics of each method (see Figure 18 in [10]). This approach involves the detection of changes in conductance across a nanowire when a charged target, such as a protein molecule, binds to it. Chua et al. employed this technique for the ultrasensitive, label-free detection of cardiac troponin-T (cTnT), a crucial biomarker for myocardial infarction. In their study, silicon nanowires were specifically functionalized with antibodies against human cTnT, enabling the detection of this protein at concentrations as low as 1 fg/mL, equivalent to 3 attomolar. This demonstrates the method's potential for highly sensitive medical diagnostics (see Figure 20 in [10]).

Comparison of SPR and LSPR for Sensing Applications

LSPR and SPR are two advanced optical sensing techniques that exploit the interaction between light and metal surfaces to detect molecular interactions. While both techniques are based on the excitation of surface plasmons, they have distinct differences in their mechanisms, instrumentation, and applications [152]. SPR occurs when polarized light strikes a metal-dielectric interface at a specific angle, leading to the excitation of surface plasmons. These plasmons are surface waves that travel along the interface. Resonance conditions in SPR require both energy and momentum matching. This necessitates the use of adaptive optics, such as prisms, to increase the momentum of the incident light to match that of the surface plasmons. LSPR occurs in metal nanoparticles when the incident light resonates with the natural frequency of the surface electrons oscillating against the restoring force of positive nuclei [152]. Unlike SPR, LSPR does not require momentum matching. Resonance is achieved by tuning the wavelength of the incident light to match the resonance frequency of the nanoparticles.

The setup for SPR is complex and requires precise alignment of optical components. A typical configuration involves a P-polarized laser light passing through an optical prism and striking the metal surface at a controlled angle. The system must maintain precise temperature control and alignment to

ensure accurate measurements, adding to the complexity and cost. LSPR instrumentation is relatively simple, often requiring only a basic light source (e.g., LEDs) and a detector (e.g., spectrometer or photodiode). The resonance condition is primarily dependent on the properties of the nanoparticles and the incident light wavelength, eliminating the need for complex optical arrangements and temperature control.

SPR can sense changes up to a micron away from the metal surface, making it sensitive to bulk refractive index changes. This large sensing volume can lead to bulk effects, where unbound biomolecules in the vicinity of the sensor surface contribute to the signal, potentially causing false positives. The propagation length of the surface plasmons in SPR can extend from a few microns to millimeters, depending on the conditions. LSPR has a much smaller sensing volume, typically extending only a few tens of nanometers from the nanoparticle surface. This localized sensing reduces the bulk effect and enhances the specificity of the sensor. The localized nature of LSPR ensures that only molecules in close proximity to the nanoparticle surface contribute to the signal, improving accuracy in detecting specific interactions.

This section provides a detailed comparison between SPR and LSPR for sensing applications. The derivation of the key equations originates from [9]. The analysis focuses on the wavelength shift in the plasmon resonance spectrum due to the adsorption of a layer with a specific thickness and refractive index.

Derivation of Key Equations

We start by considering the shift in the LSPR due to the adsorption of a layer of thickness d and refractive index n_A onto the nanoparticle surface [9]. The refractive index at distances greater than d from the nanoparticle surface is assumed to be n_E. The distance-dependent refractive index $n(z)$ can be expressed as follows:

$$n(z) = \begin{cases} n_A & \text{for } 0 \le z \le d \\ n_E & \text{for } d < z < \infty \end{cases} \tag{45}$$

The wavelength shift $\Delta\lambda$ in the LSPR spectrum due to the introduction of the adsorption layer is given by the following:

$$\Delta\lambda = m(n_{\text{final}} - n_{\text{initial}}) \tag{46}$$

where m is the bulk refractive index sensitivity of the nanoparticles, $n_{\text{initial}} = n_E$, and n_{final} is the effective refractive index due to the combination of the adsorbed layer and the external environment. To account for the distance-dependent intensity of the electromagnetic (EM) field, which decays exponentially with a characteristic length l_d, we approximate the EM field as follows:

$$E(z) = E_0 \exp\left(-\frac{z}{l_d}\right) \tag{47}$$

The effective refractive index n_{eff} is normalized by the intensity factor, leading to the following expression:

$$n_{\text{eff}} = \int_0^\infty n(z) \exp\left(-\frac{2z}{l_d}\right) dz \Big/ \int_0^\infty \exp\left(-\frac{2z}{l_d}\right) dz \tag{48}$$

Substituting $n(z)$ and evaluating the integrals, we get the following:

$$n_{\text{eff}} = n_A \left(1 - \exp\left(-\frac{2d}{l_d}\right)\right) + n_E \exp\left(-\frac{2d}{l_d}\right) \tag{49}$$

Inserting n_{eff} into the expression for $\Delta\lambda$, we obtain the following:

$$\Delta\lambda = m(n_{\text{eff}} - n_E) \tag{50}$$

$$= m\left[n_A \left(1 - \exp\left(-\frac{2d}{l_d}\right)\right) + n_E \exp\left(-\frac{2d}{l_d}\right) - n_E\right] \tag{51}$$

Simplifying, we derive the following:

$$\Delta\lambda = m(n_A - n_E)\left(1 - \exp\left(-\frac{2d}{l_d}\right)\right) \tag{52}$$

This equation reduces to $\Delta\lambda = m(n_A - n_E)$ in bulk solvents where d approaches infinity. This approach also applies to multilayer systems as shown in the referenced works.

Direct Comparison of SPR and LSPR

We can use this equation to compare the performance of SPR and LSPR sensors. The ratio of the wavelength shifts for LSPR and SPR is given by the following:

$$\frac{\Delta\lambda_{\text{LSPR}}}{\Delta\lambda_{\text{SPR}}} = \frac{m_{\text{LSPR}}\left(1 - \exp\left(-\frac{2d}{l_{d,\text{LSPR}}}\right)\right)}{m_{\text{SPR}}\left(1 - \exp\left(-\frac{2d}{l_{d,\text{SPR}}}\right)\right)} \tag{53}$$

Given $m_{\text{SPR}} = 9000\,\text{nm/RIU}$, $m_{\text{LSPR}} = 200\,\text{nm/RIU}$, $l_{d,\text{SPR}} = 200\,\text{nm}$, and $l_{d,\text{LSPR}} = 5\,\text{nm}$, we can directly compare the sensors' performance. This comparison shows that while SPR sensors outperform LSPR sensors for bulk refractive index changes by a factor of 45, their performance is comparable for thin adsorption layers due to the

short EM-field decay length in LSPR sensors. Additionally, considering the surface areas of the substrates, an SPR thin film occupies more area than a nanoparticle array used in LSPR. For instance, in a 10×10 μm region, nanoparticles occupy only 9.7% of the area compared to a continuous thin film. Therefore, LSPR sensors outperform SPR sensors in terms of the wavelength-shift response per adsorbed molecule, making them advantageous for sensing applications with small concentrations, including single-molecule detection. While SPR sensors are more sensitive to bulk refractive index changes, LSPR sensors provide comparable performance for thin adsorption layers and superior performance per adsorbed molecule. This makes LSPR sensors highly suitable for applications requiring high sensitivity to small molecular interactions.

SPR is widely used in various biosensing applications, particularly where larger sensing volumes are advantageous. However, the bulk effect and the need for complex instrumentation limit its applicability in some diagnostics, especially in complex matrices like blood. LSPR is particularly suited for applications requiring high specificity and minimal bulk effect, such as in vitro diagnostics. Its simpler instrumentation and reduced sensitivity to bulk refractive index changes make it ideal for detecting low-abundance biomarkers in complex samples like serum, plasma, or saliva. The flexibility and scalability of LSPR technology also make it suitable for developing portable, point-of-care diagnostic devices.

Challenges and Opportunities in the Development of LSPR

Challenges

LSPR-based sensors are highly sensitive to changes in the local dielectric environment, which is advantageous for detection. However, this sensitivity also presents challenges, particularly when external factors such as temperature fluctuations, pH variations, or nonspecific binding events can introduce noise and affect the accuracy and reliability of measurements. Ensuring the reproducibility of LSPR signals in complex biological samples remains a significant challenge, necessitating the development of more robust surface functionalization strategies and real-time compensation mechanisms. The fabrication of nanostructures for LSPR applications requires precise control over size, shape, and material composition to ensure consistent plasmonic responses. Current fabrication techniques, such as electron beam lithography and nanosphere lithography, while advanced, often suffer from scalability issues, high costs, and potential batch-to-batch variations. These limitations can hinder the mass production of LSPR-based devices and affect their widespread adoption in commercial applications.

While LSPR is qualitative in detecting the presence of analytes, quantification remains challenging, particularly at low concentrations. Developing standardized protocols for the quantitative analysis of LSPR signals is crucial for its integration into routine analytical workflows. This requires addressing issues related to signal amplification, baseline drift, and the development of universal calibration standards. The interpretation of LSPR data, particularly in multiplexed assays, can be complex due to overlapping plasmonic signals and the influence of multiple variables on the resonance peak. Advanced data analysis techniques, such as machine learning algorithms, are increasingly being employed to deconvolute these signals, but their integration into user-friendly platforms is still in the early stages. The choice of materials for LSPR sensors is often limited to noble metals like gold and silver, which exhibit desirable plasmonic properties but also have drawbacks, such as susceptibility to oxidation (in the case of silver) and limited tunability in the visible and near-infrared regions. Exploring alternative materials or composite nanostructures that can overcome these limitations while maintaining strong plasmonic responses is a critical area of ongoing research.

Opportunities

The development of more sophisticated and scalable nanofabrication techniques, such as nanoimprint lithography and self-assembly methods, presents opportunities to produce LSPR-active nanostructures with greater uniformity and at lower costs. These advancements could facilitate the commercialization of LSPR-based sensors and devices, making them more accessible for a range of applications, from clinical diagnostics to environmental monitoring. The integration of LSPR sensors with microfluidic platforms offers significant opportunities for enhancing the performance of biosensors. Microfluidics enables precise control over sample flow, minimizes reagent consumption, and allows for the development of portable, lab-on-a-chip devices. This integration could lead to the creation of highly sensitive, real-time diagnostic tools that can be deployed in point-of-care settings.

Innovations in surface chemistry and receptor engineering are expanding the range of analytes that can be detected using LSPR, including small molecules, viruses, and nucleic acids. The development of new recognition elements, such as aptamers and molecularly imprinted polymers, offers the potential to improve the selectivity and sensitivity of LSPR sensors, broadening their applicability in diverse fields such as medical diagnostics, food safety, and environmental monitoring. The application of computational methods, including finite-difference time-domain (FDTD) simulations and machine learning, to the design and optimization of LSPR systems represents a significant opportunity. These

methods can accelerate the discovery of new nanostructures with optimized plasmonic properties and facilitate the real-time analysis of complex LSPR data, making these systems more versatile and easier to use. Beyond sensing applications, the unique optical properties of LSPR-active nanoparticles are being explored for therapeutic applications, particularly in plasmonic photothermal therapy. This technique leverages the ability of nanoparticles to convert light into heat, offering a targeted approach to treat cancer and other diseases. The ongoing research into biocompatible and tunable LSPR materials could open up new avenues for combined diagnostic and therapeutic (theranostic) applications.

Recent Developments in Nanoparticle Fabrication, LSPR Sensors in Novel Applications, and Innovations in LSPR Modulation Using External Stimuli

In the last decade, significant progress has been made in the controlled synthesis of nanoparticles, focusing on tailoring their shapes and materials to enhance LSPR sensitivity. Advances in chemical and green synthesis methods have allowed for precise control over nanoparticle size and morphology, including the production of nanostructures such as nanostars, nanocubes, and bipyramids [153–157]. These shapes, due to their sharp tips and high aspect ratios, exhibit stronger electric field enhancements, making them particularly effective for LSPR sensing applications. Techniques such as seed-mediated growth and lithography have become more refined, offering higher reproducibility in nanoparticle fabrication [158]. Hybrid nanoparticles, combining different metals (e.g., gold-silver alloys), have also emerged, demonstrating improved plasmonic properties by tuning their composition to achieve desired optical properties. Bottom-up approaches, including self-assembly techniques and wet chemical methods, have become critical in achieving nanoparticles with consistent shape and size, essential for ensuring high sensitivity in LSPR-based detection systems [159–161].

Recent developments have seen LSPR sensors integrated with other modalities, such as Raman spectroscopy, to create powerful hybrid sensing systems. One notable combination is LSPR with surface-enhanced Raman spectroscopy (SERS), which has allowed for the detection of extremely low analyte concentrations due to the enhanced electromagnetic fields generated near the nanoparticle surface [162–164]. This hybrid system is particularly valuable in biosensing, where it enables the detection of biomolecules at trace levels with high sensitivity and specificity. Another novel application is the use of multiplexed biosensing platforms, where multiple LSPR sensors are employed simultaneously for real-time, high-throughput detection of various biomarkers in medical diagnostics. This integration of LSPR with multiplexing and real-time monitoring technologies is proving to be transformative in fields such as environmental monitoring and healthcare.

LSPR sensors have seen remarkable advancements through the modulation of nanoparticle properties using external stimuli like light, temperature, and electric fields. For instance, temperature-responsive LSPR sensors have been developed, where changes in temperature can induce shifts in the plasmonic response, enhancing the sensor's ability to detect temperature-sensitive biological interactions [165]. Similarly, electric fields have been utilized to actively tune the refractive index sensitivity of nanoparticles, allowing for real-time control of the LSPR signal [166]. This is particularly useful in dynamic sensing environments, where continuous monitoring and modulation of the sensor's response are necessary for accurate detection. Light-driven assembly and disassembly of nanoparticle clusters have also been demonstrated, offering a reversible means to control LSPR properties for enhanced sensing performance [166].

The development of metamaterials has opened new possibilities for enhancing LSPR sensitivity and tunability [167–170]. Metamaterials, engineered to exhibit unique refractive index properties, have been used to create LSPR sensors with a wider spectral response and higher sensitivity [171]. These materials allow for the coupling of plasmonic resonances at nanoscale dimensions, enabling LSPR sensors to achieve superior performance, particularly in detecting subtle changes in the surrounding environment. Another emerging trend is the combination of LSPR with fluorescence-based detection systems, forming hybrid sensors capable of dual-modality detection [172]. These systems leverage the strengths of both LSPR and fluorescence, allowing for enhanced detection sensitivity and extended dynamic ranges. Hybrid LSPR-fluorescence sensors are particularly promising for applications requiring real-time, in-situ monitoring of biomolecular interactions, such as in complex biological environments.

Conclusion

LSPR has emerged as a powerful tool in the realm of nanoscale sensing, offering precise detection capabilities through the interaction of light with noble metal nanoparticles. This review highlights significant advancements in the fabrication and application of LSPR-based sensors, emphasizing the underlying physical principles and theoretical models. By examining various nanoparticle shapes, sizes, and compositions, the paper underscores the versatility and potential of LSPR in biological and chemical sensing. The comprehensive analysis presented herein not only elucidates

the current state of LSPR technology but also paves the way for future innovations in sensor design and application. With continued research and development, LSPR sensors hold the promise of becoming indispensable tools in both scientific research and practical diagnostics.

Author Contribution M.M., K.M., and M.S. contributed to the writing and review of this article. P.M. contributed to the review of the article.

Funding Open access funding provided by Council for Scientific and Industrial Research. This research was supported by the CSIR and DSI. K.M. was also supported by the South African Quantum Technology Initiative (SAQuTi) and the South African Medical Research Council (SAMRC).

Data Availability No datasets were generated or analysed during the current study.

Declarations

Competing interests The authors declare no competing interests.

References

1. Adhikari S, Spaeth P, Kar A, Baaske MD, Khatua S, Orrit M (2020) Photothermal microscopy: imaging the optical absorption of single nanoparticles and single molecules. ACS nano 14(12):16 414–16 445
2. Chen LK (2019) Dementia care in developing countries. Aging Med Healthcare 4:120–121
3. Das AJ, Shivanna R, Narayan K (2014) Photoconductive NSOM for mapping optoelectronic phases in nanostructures. Nanophotonics 3(1–2):19–31
4. Denkova D, Verellen N, Silhanek AV, Valev VK, Dorpe PV, Moshchalkov VV (2013) Mapping magnetic near-field distributions of plasmonic nanoantennas. ACS nano 7(4):3168–3176
5. Brolo AG, Kwok SC, Moffitt MG, Gordon R, Riordon J, Kavanagh KL (2005) Enhanced fluorescence from arrays of nanoholes in a gold film. J Am Chemical Soc 127(42):14 936–14 941
6. Albella P, Alcaraz de la Osa R, Moreno F, Maier SA (2014) Electric and magnetic field enhancement with ultralow heat radiation dielectric nanoantennas: considerations for surface-enhanced spectroscopies. Acs Photonics 1(6):524–529
7. Rivera V, Ferri F, Marega E Jr (2012) Localized surface plasmon resonances: noble metal nanoparticle interaction with rare-earth ions. Plasmonics-Principles Appl 1(11):283–312
8. Halas NJ, Lal S, Chang W-S, Link S, Nordlander P (2011) Plasmons in strongly coupled metallic nanostructures. Chemical Rev 111(6):3913–3961
9. Willets DG (2023) Advances in plasmonic surface-enhanced Raman spectroscopy. Annual Rev Physical Chemistry 58(1):267–297. [Online]. Available: https://www.annualreviews.org/docserver/fulltext/pc/58/1/pc.57.willets.pdf?expires=1718899132&id=id&accname=guest&checksum=F80F620B39AD1A5BC3CE6CD90E963879
10. Mayer KM, Hafner JH (2011) Localized surface plasmon resonance sensors. Chemical Rev 111(6):3828–3857
11. Willets KA, Van Duyne RP (2007) Localized surface plasmon resonance spectroscopy and sensing. Annu Rev Phys Chem 58:267–297
12. Fan X, Zheng W, Singh DJ (2014) Light scattering and surface plasmons on small spherical particles. Light: Sci Appl 3(6):e179–e179
13. Wriedt T (2012) Mie theory: a review. Basics and applications, The Mie theory, pp 53–71
14. Mie G (1908) Contribution to the optic of turbid media, especially colloidal metal solutions. Annalen der Physik 25:3
15. Bohren CF, Huffman DR (2008) Absorption and scattering of light by small particles. John Wiley & Sons
16. Nusz GJ, Marinakos SM, Curry AC, Dahlin A, Höök F, Wax A, Chilkoti A (2008) Label-free plasmonic detection of biomolecular binding by a single gold nanorod. Analytical Chem 80(4):984–989
17. Rv Gans (1912) The shape of ultra microscopic gold particles. Ann Phys 37(881):422
18. Alekseeva A, Bogatyrev V, Khlebtsov B, Mel'Nikov A, Dykman L, Khlebtsov N (2006) Gold nanorods: synthesis and optical properties. Colloid J 68:661–678
19. Anderson LJ, Mayer KM, Fraleigh RD, Yang Y, Lee S, Hafner JH (2010) Quantitative measurements of individual gold nanoparticle scattering cross sections. J Phys Chemistry C 114(25):11 127–11 132
20. Faraday M (1964) Faraday. In: A History of Chemistry. Springer, pp 99–141
21. Gans R (1912) Über die form ultramikroskopischer goldteilchen. Annalen der Physik 342(5):881–900
22. Zhao J, Pinchuk AO, McMahon JM, Li S, Ausman LK, Atkinson AL, Schatz GC (2008) Methods for describing the electromagnetic properties of silver and gold nanoparticles. Accounts Chem Res 41(12):1710–1720
23. Joyce C, Fothergill S, Xie F (2020) Recent advances in gold-based metal enhanced fluorescence platforms for diagnosis and imaging in the near-infrared. Mater Today Adv 7:100073
24. Lee SH, Jun B-H (2019) Silver nanoparticles: synthesis and application for nanomedicine. Int J Molecular Sci 20(4):865
25. Kang S-M (2022) Study of optical information recording mechanism based on localized surface plasmon resonance with Au nanoparticles array deposited media and ridge-type nanoaperture. Nanomaterials 12(8):1350
26. Khan I, Saeed K, Khan I (2019) Nanoparticles: properties, applications and toxicities. Arabian J Chem 12(7):908–931
27. Demishkevich E, Zyubin A, Seteikin A, Samusev I, Park I, Hwangbo CK, Choi EH, Lee GJ (2023) Synthesis methods and optical sensing applications of plasmonic metal nanoparticles made from rhodium, platinum, gold, or silver. Materials 16(9):3342
28. Petryayeva E, Krull UJ (2011) Localized surface plasmon resonance: nanostructures, bioassays and biosensing–a review. Analytica Chimica Acta 706(1):8–24

29. Liu Q-m, Zhou D-b, Yamamoto Y, Ichino R, Okido M (2012) Preparation of Cu nanoparticles with NaBH4 by aqueous reduction method. Trans Nonferrous Metals Soc China 22(1):117–123
30. Mourdikoudis S, Pallares RM, Thanh NT (2018) Characterization techniques for nanoparticles: comparison and complementarity upon studying nanoparticle properties. Nanoscale 10(27):12 871–12 934
31. Sepúlveda B, Angelomé PC, Lechuga LM, Liz-Marzán LM (2009) LSPR-based nanobiosensors. Nano Today 4(3):244–251
32. Ealia SAM, Saravanakumar MP (2017) A review on the classification, characterisation, synthesis of nanoparticles and their application. In: *IOP conference series: materials science and engineering* 263(3). IOP Publishing, pp 032019
33. Ijaz I, Gilani E, Nazir A, Bukhari A (2020) Detail review on chemical, physical and green synthesis, classification, characterizations and applications of nanoparticles. Green Chemistry Lett Rev 13(3):223–245
34. Gunasekaran K, Nirmala M, Raja K, Saravanakumar A (2017) Characterization and application of biosynthesized silver nanoparticles from Melia dubia leaves
35. Helmlinger J, Prymak O, Loza K, Gocyla M, Heggen M, Epple M (2016) On the crystallography of silver nanoparticles with different shapes. Crystal Growth Design 16(7):3677–3687
36. Edwards AA, Alexander BD (2017) UV-visible absorption spectroscopy, organic applications
37. Pal A, Saha S, Kumar Maji S, Kundu M, Kundu A (2012) Wet-chemical synthesis of spherical arsenic nanoparticles by a simple reduction method and its characterization. Adv Mater Lett 3(3):177–180
38. Chaki S, Malek TJ, Chaudhary M, Tailor J, Deshpande M (2015) Magnetite Fe3O4 nanoparticles synthesis by wet chemical reduction and their characterization. Adv Natural Sci: Nanosci Nanotechnol 6(3):035009
39. Shameli K, Ahmad MB, Yunus WZW, Ibrahim NA, Darroudi M (2010) Synthesis and characterization of silver/talc nanocomposites using the wet chemical reduction method. Int J Nanomed pp 743–751
40. Hiep HM, Nakayama T, Saito M, Yamamura S, Takamura Y, Tamiya E (2008) A microfluidic chip based on localized surface plasmon resonance for real-time monitoring of antigen-antibody reactions. Japanese J Appl Phys 47(2S):1337
41. dos Santos SS, P, MMM de Almeida J, Pastoriza-Santos I, CC Coelho L, (2021) Advances in plasmonic sensing at the NIR–a review. Sensors 21(6):2111
42. Le Ru E, Etchegoin P (2008) Principles of surface-enhanced Raman spectroscopy: and related plasmonic effects. Elsevier
43. Malinsky MD, Kelly KL, Schatz GC, Van Duyne RP (2001) Chain length dependence and sensing capabilities of the localized surface plasmon resonance of silver nanoparticles chemically modified with alkanethiol self-assembled monolayers. J Am Chemical Soc 123(7):1471–1482
44. Haes AJ, Zou S, Schatz GC, Van Duyne RP (2004) Nanoscale optical biosensor: short range distance dependence of the localized surface plasmon resonance of noble metal nanoparticles. J Physical Chemistry B 108(22):6961–6968
45. Nusz GJ, Curry AC, Marinakos SM, Wax A, Chilkoti A (2009) Rational selection of gold nanorod geometry for label-free plasmonic biosensors. ACS nano 3(4):795–806
46. Becker J, Trügler A, Jakab A, Hohenester U, Sönnichsen C (2010) The optimal aspect ratio of gold nanorods for plasmonic biosensing. Plasmonics 5:161–167
47. Abrica-González P, Zamora-Justo J, Chavez-Sandoval BE, Vázquez-Martínez G, Balderas-López J (2018) Measurement of the optical properties of gold colloids by photoacoustic spectroscopy. Int J Thermophys 39:1–7
48. Sun Y, Xia Y (2002) Increased sensitivity of surface plasmon resonance of gold nanoshells compared to that of gold solid colloids in response to environmental changes. Analytical Chemistry 74(20):5297–5305
49. Link S, El-Sayed MA (1999) Spectral properties and relaxation dynamics of surface plasmon electronic oscillations in gold and silver nanodots and nanorods. pp 8410–8426
50. Henzie J, Lee MH, Odom TW (2007) Multiscale patterning of plasmonic metamaterials. Nature Nanotechnol 2(9):549–554
51. Liu N, Weiss T, Mesch M, Langguth L, Eigenthaler U, Hirscher M, Sonnichsen C, Giessen H (2010) Planar metamaterial analogue of electromagnetically induced transparency for plasmonic sensing. Nano Lett 10(4):1103–1107
52. Dmitriev A, Hägglund C, Chen S, Fredriksson H, Pakizeh T, Käll M, Sutherland DS (2008) Enhanced nanoplasmonic optical sensors with reduced substrate effect. Nano Lett 8(11):3893–3898
53. Shen J, Luan B, Pei H, Yang Z, Zuo X, Liu G, Shi J, Wang L, Zhou R, Cheng W et al (2017) Humidity-responsive single-nanoparticle-layer plasmonic films. Advanced Mater 29(35):1606796
54. Li J, Jia X (2023) Photo-controlled self-assembly of nanoparticles: a promising strategy for development of novel structures. Nanomaterials 13(18):2562
55. Yeshchenko O, Bondarchuk I, Gurin V, Dmitruk I, Kotko A (2013) Temperature dependence of the surface plasmon resonance in gold nanoparticles. Surface Sci 608:275–281
56. Wang L, Zare D, Chow TH, Wang J, Magnozzi M, Chergui M (2022) Disentangling light-and temperature-induced thermal effects in colloidal au nanoparticles. J Physical Chemistry C 126(7):3591–3599
57. Guidi L, Cascone MG, Rosellini E (2024) Light-responsive polymeric nanoparticles for retinal drug delivery: design cues, challenges and future perspectives. Heliyon
58. Loiseau A, Asila V, Boitel-Aullen G, Lam M, Salmain M, Boujday S (2019) Silver-based plasmonic nanoparticles for and their use in biosensing. Biosensors 9(2):78
59. Dong X, Ji X, Wu H, Zhao L, Li J, Yang W (2009) Shape control of silver nanoparticles by stepwise citrate reduction. J Physical Chemistry C 113(16):6573–6576
60. Mukherji S, Bharti S, Shukla G, Mukherji S (2019) Synthesis and characterization of size-and shape-controlled silver nanoparticles. Physical Sci Rev 4(1):20170082
61. Riswan M, Adrianto N, Yahya IM, Istiqomah NI, Panre AM, Wahyuni S, Arifin M, Santoso I, Suharyadi E et al (2023) Effect of electric field on localized surface plasmon resonance properties of Fe3O4/Ag composite nanoparticles. Optik 293:171404
62. Riswan M, Widianto E, Istiqomah NI, Driyo C, Arifin M, Santoso I, Suharyadi E (2024) Tuning optical properties of Au thin film using electric field for surface plasmon resonance biosensor application. Optical Mater 150:115221
63. Gautam A, Komal P, Gautam P, Sharma A, Kumar N, Jung JP (2021) Recent trends in noble metal nanoparticles for colorimetric chemical sensing and micro-electronic packaging applications. Metals 11(2):329
64. Fiammengo R (2017) Can nanotechnology improve cancer diagnosis through miRNA detection? Biomarkers Med 11(1):69–86
65. Ehuwa O, Jaiswal AK, Jaiswal S (2021) Salmonella, food safety and food handling practices. Foods 10(5):907
66. Fleischer M (2012) Near-field scanning optical microscopy nanoprobes. Nanotechnol Rev 1(4):313–338
67. Kelly J, Keegan G, Brennan-Fournet M (2012) Triangular silver nanoparticles: their preparation, functionalisation and properties. Acta Physica Polonica A 122(2):337–345
68. Kim H-M, Kim H-J, Park J-H, Lee S-K (2022) High-performance biosensor using a sandwich assay via antibody-conjugated gold

nanoparticles and fiber-optic localized surface plasmon resonance. Analytica Chimica Acta 1213:339960
69. Betzig E, Trautman JK (1992) Near-field optics: microscopy, spectroscopy, and surface modification beyond the diffraction limit. Science 257(5067):189–195
70. Wang Z, Wang X, Cong S, Chen J, Sun H, Chen Z, Song G, Geng F, Chen Q, Zhao Z (2020) Towards full-colour tunability of inorganic electrochromic devices using ultracompact fabry-perot nanocavities. Nat Commun 11(1):302
71. Greffet J-J, Carminati R (1997) Image formation in near-field optics. Progress Surface Sci 56(3):133–237
72. Sönnichsen C, Franzl T, Wilk T, von Plessen G, Feldmann J, Wilson O, Mulvaney P (2002) Drastic reduction of plasmon damping in gold nanorods. Physical Rev Lett 88(7):077402
73. Hartland GV (2011) Optical studies of dynamics in noble metal nanostructures. Chem Rev 111(6):3858–3887
74. Sreeprasad TS, Pradeep T (2013) Noble metal nanoparticles. Springer Handbook Nanomater 303–388
75. Singh VK, Sharma N, Singh VK (2022) Application of x-ray fluorescence spectrometry in plant science: Solutions, threats, and opportunities. X-Ray Spectrometry 51(3):304–327
76. Sönnichsen C, Reinhard BM, Liphardt J, Alivisatos AP (2005) A molecular ruler based on plasmon coupling of single gold and silver nanoparticles. Nature Biotechnol 23(6):741–745
77. Calvo R, Pini V, Thon A, Saad A, Salvador-Matar A, Manso Silván M, Ahumada Ó (2023) Amplitude-resolved single particle spectrophotometry: a robust tool for high-throughput size characterization of plasmonic nanoparticles. Nanomaterials 13(17):2401
78. Wang S-H, Kuo C-W, Lo S-C, Yeung WK, Chang T-W, Wei P-K (2022) Spectral image contrast-based flow digital nanoplasmonmetry for ultrasensitive antibody detection. J Nanobiotechnol 20(1):6
79. Gahlaut SK, Pathak A, Gupta BD (2022) Recent advances in silver nanostructured substrates for plasmonic sensors. Biosensors 12(9):713
80. Stewart ME, Anderton CR, Thompson LB, Maria J, Gray SK, Rogers JA, Nuzzo RG (2008) Nanostructured plasmonic sensors. Chemical Rev 108(2):494–521
81. Ruemmele JA, Hall WP, Ruvuna LK, Van Duyne RP (2013) A localized surface plasmon resonance imaging instrument for multiplexed biosensing. Analytical Chemistry 85(9):4560–4566
82. Raphael MP, Christodoulides JA, Mulvaney SP, Miller MM, Long JP, Byers JM (2012) A new methodology for quantitative lspr biosensing and imaging. Analytical Chem 84(3):1367–1373
83. Haes AJ, Zou S, Zhao J, Schatz GC, Van Duyne RP (2006) Localized surface plasmon resonance spectroscopy near molecular resonances. J American Chem Soc 128(33):10 905–10 914
84. Tessaro L, Aquino A, de Carvalho APA, Conte-Junior CA (2021) A systematic review on gold nanoparticles based-optical biosensors for influenza virus detection. Sensors Actuators Reports 3:100060
85. Moulick A, Richtera L, Milosavljevic V, Cernei N, Haddad Y, Zitka O, Kopel P, Heger Z, Adam V (2017) Advanced nanotechnologies in avian influenza: current status and future trends-a review. Analytica Chimica Acta 983:42–53
86. Yoo SY, Kim D-K, Park TJ, Kim EK, Tamiya E, Lee SY (2010) Detection of the most common corneal dystrophies caused by bigh3 gene point mutations using a multispot gold-capped nanoparticle array chip. Analytical Chem 82(4):1349–1357
87. Chen C-D, Cheng S-F, Chau L-K, Wang CC (2007) Sensing capability of the localized surface plasmon resonance of gold nanorods. Biosensors Bioelectron 22(6):926–932
88. Rindzevicius T, Alaverdyan Y, Dahlin A, Höök F, Sutherland DS, Käll M (2005) Plasmonic sensing characteristics of single nanometric holes. Nano Lett 5(11):2335–2339
89. Pironti C, Ricciardi M, Proto A, Bianco PM, Montano L, Motta O (2021) Endocrine-disrupting compounds: An overview on their occurrence in the aquatic environment and human exposure. Water 13(10):1347
90. Lee K-S, El-Sayed MA (2006) Gold and silver nanoparticles in sensing and imaging: sensitivity of plasmon response to size, shape, and metal composition. J Physical Chem B 110(39):19 220–19 225
91. Park TJ, Lee SJ, Kim D-K, Heo NS, Park JY, Lee SY (2012) Development of label-free optical diagnosis for sensitive detection of influenza virus with genetically engineered fusion protein. Talanta 89:246–252
92. Xu T, Geng Z (2021) Strategies to improve performances of lspr biosensing: Structure, materials, and interface modification. Biosensors Bioelectron 174:112850
93. Li S, Fang Y, Wang J (2024) Control of light–matter interactions in two-dimensional materials with nanoparticle-on-mirror structures. Opto-Electronic Sci 3(7):240 011–1
94. Xu J, Wu Y, Zhang P, Wu Y, Vallée RA, Wu S, Liu X (2021) Resonant scattering manipulation of dielectric nanoparticles. Adv Optical Mater 9(15):2100112
95. Dutta R, Singh BP, Kundu T (2013) Plasmonic coupling effect on spectral response of silver nanoparticles immobilized on an optical fiber sensor. J Physical Chem C 117(33):17 167–17 176
96. Sapsford KE, Algar WR, Berti L, Gemmill KB, Casey BJ, Oh E, Stewart MH, Medintz IL (2013) Functionalizing nanoparticles with biological molecules: developing chemistries that facilitate nanotechnology. Chem Rev 113(3):1904–2074
97. Hoener BS, Kirchner SR, Heiderscheit TS, Collins SS, Chang W-S, Link S, Landes CF (2018) Plasmonic sensing and control of single-nanoparticle electrochemistry. Chem 4(7):1560–1585
98. Gellé A, Moores A (2017) Water splitting catalyzed by titanium dioxide decorated with plasmonic nanoparticles. Pure Appl Chem 89(12):1817–1827
99. Dubas ST, Pimpan V (2008) Green synthesis of silver nanoparticles for ammonia sensing. Talanta 76(1):29–33
100. Choi Y, Park Y, Kang T, Lee LP (2009) Selective and sensitive detection of metal ions by plasmonic resonance energy transfer-based nanospectroscopy. Nat Nanotechnol 4(11):742–746
101. Endo T, Kerman K, Nagatani N, Hiepa HM, Kim D-K, Yonezawa Y, Nakano K, Tamiya E (2006) Multiple label-free detection of antigen- antibody reaction using localized surface plasmon resonance-based core- shell structured nanoparticle layer nanochip. Analytical Chem 78(18):6465–6475
102. Yu C, Nakshatri H, Irudayaraj J (2007) Identity profiling of cell surface markers by multiplex gold nanorod probes. Nano Lett 7(8):2300–2306
103. Wang C, Irudayaraj J (2008) Gold nanorod probes for the detection of multiple pathogens. Birck NCN Publications, pp 397
104. Yu C, Irudayaraj J (2007) Multiplex biosensor using gold nanorods. Analytical Chem 79(2):572–579
105. Yonzon CR, Jeoung E, Zou S, Schatz GC, Mrksich M, Van Duyne RP (2004) A comparative analysis of localized and propagating surface plasmon resonance sensors: the binding of concanavalin a to a monosaccharide functionalized self-assembled monolayer. J Am Chem Soc 126(39):12 669–12 676
106. Bingham JM, Willets KA, Shah NC, Andrews DQ, Van Duyne RP (2009) Localized surface plasmon resonance imaging: simultaneous single nanoparticle spectroscopy and diffusional dynamics. J Physical Chem C 113(39):16 839–16 842
107. Bhalla N, Shen AQ (2024) Localized surface plasmon resonance sensing and its interplay with fluidics. Langmuir 40(19):9842–9854
108. Cheng S-F, Chau L-K (2003) Colloidal gold-modified optical fiber for chemical and biochemical sensing. Analytical Chem 75(1):16–21

109. Mitsui K, Handa Y, Kajikawa K (2004) Optical fiber affinity biosensor based on localized surface plasmon resonance. Appl Phys Lett 85(18):4231–4233
110. Tang J-L, Cheng S-F, Hsu W-T, Chiang T-Y, Chau L-K (2006) Fiber-optic biochemical sensing with a colloidal gold-modified long period fiber grating. Sensors and Actuators B: Chemical 119(1):105–109
111. Shao Y, Xu S, Zheng X, Wang Y, Xu W (2010) Optical fiber lspr biosensor prepared by gold nanoparticle assembly on polyelectrolyte multilayer. Sensors 10(4):3585–3596
112. Kelly KL, Coronado E, Zhao LL, Schatz GC (2003) The optical properties of metal nanoparticles: the influence of size, shape, and dielectric environment. pp 668–677
113. Ourir A, Fink M (2014) Subwavelength far-field imaging at visible and ultraviolet wavelengths using broadband surface plasmon waves. Phys Rev B 89(11):115403
114. Querebillo CJU (2020) Combined vibrational spectroscopy and electrochemistry for studying biological and materials systems. Ph.D. dissertation, Dissertation, Berlin, Technische Universität Berlin, 2019
115. Mcoyi M, Lugongolo M, Williamson C, Mpofu K, Mthunzi-Kufa P (2024) Detection of mutations using a localized surface plasmon resonance biosensor. In: Optical Interactions with Tissue and Cells XXXV, vol. 12840. SPIE, 2024, pp 62–68
116. Rajeshwari A, Karthiga D, Chandrasekaran N, Mukherjee A (2016) Anti-aggregation-based spectrometric detection of hg (ii) at physiological ph using gold nanorods. Materials Science and Engineering: C 67:711–716
117. Lee J, Jeon D-J, Yeo J-S (2021) Quantum plasmonics: energy transport through plasmonic gap. Adv Mater 33(47):2006606
118. Naumov AV, Gorshelev AA, Vainer YG, Kador L, Köhler J (2009) Far-field nanodiagnostics of solids with visible light by spectrally selective imaging. Angewandte Chemie International Edition 48(51):9747–9750
119. McFarland AD, Van Duyne RP (2003) Single silver nanoparticles as real-time optical sensors with zeptomole sensitivity. Nano Lett 3(8):1057–1062
120. Jáuregui-López I, Rodríguez-Ulibarri P, Urrutia A, Kuznetsov SA, Beruete M (2018) Labyrinth metasurface absorber for ultra-high-sensitivity terahertz thin film sensing. Physica status solidi (RRL)–Rapid Research Letters 12(10):1800375
121. Alipour A, Farmani A, Mir A (2018) High sensitivity and tunable nanoscale sensor based on plasmon-induced transparency in plasmonic metasurface. IEEE Sensors J 18(17):7047–7054
122. Alsayed AE, Ghanim AM, Yahia A, Swillam MA (2023) Giant localized electromagnetic field of highly doped silicon plasmonic nanoantennas. Scientific Reports 13(1):5793
123. Cui F, Yue Y, Zhang Y, Zhang Z, Zhou HS (2020) Advancing biosensors with machine learning. ACS Sensors 5(11):3346–3364
124. Zhang K, Wang J, Liu T, Luo Y, Loh XJ, Chen X (2021) Machine learning-reinforced noninvasive biosensors for healthcare. Adv Healthcare Mater 10(17):2100734
125. Raji H, Tayyab M, Sui J, Mahmoodi SR, Javanmard M (2022) Biosensors and machine learning for enhanced detection, stratification, and classification of cells: A review. Biomed Microdevices 24(3):26
126. Tsebesebe N, Mpofu K, Ndlovu S, Sivarasu S, Mthunzi-Kufa P (2023) Detection of sars-cov-2 from raman spectroscopy data using machine learning models. MATEC Web of Conferences, vol. 388, pp 07002. [Online]. Available: https://doi.org/10.1051/matecconf/202338807002
127. Mpofu K, Lee C, Maguire G, Kruger H, Tame M (2022) Experimental measurement of kinetic parameters using quantum plasmonic sensing. J Appl Phys 131(8):
128. Mpofu KT (2020) Quantum plasmonic sensing with application to hiv research. Ph.D. dissertation
129. Mpofu K, Lee C, Maguire G, Kruger H, Tame M (2022) Measuring kinetic parameters using quantum plasmonic sensing. Physical Rev A 105(3):032619
130. Mpofu K, Ombinda-Lemboumba S (2023) Mthunzi-Kufa P (2023) Classical and quantum surface plasmon resonance biosensing. Int J Optics 1:5538161
131. Mpofu K, Mthunzi-Kufa P (2023) Quantum phase-based plasmonic biosensing for enhanced covid-19 detection. In: The 67th Annual Conference of the South African Institute of Physics (SAIP), 67(23):288–296
132. Mpofu K, Mthunzi-Kufa P (2023) Enhanced signal-to-noise ratio in quantum plasmonic image sensing including loss and varying photon number. Physica Scripta 98(11):115115
133. Mpofu KT, Mthunzi-Kufa P (2024) Quantum enhancement in the limit of detection measurement of a phase-based plasmonic biosensor including loss. In: Quantum effects and measurement techniques in biology and biophotonics, vol. 12863. SPIE, pp 8–16
134. Mpofu KT, Mthunzi-Kufa P (2024) Comparing amplitude-based and phase-based quantum plasmonic biosensing. In: Quantum effects and measurement techniques in biology and biophotonics, vol. 12863. SPIE, pp 114–121
135. Mpofu KT, Mthunzi-Kufa P (2023) Application of quantum computers to phase-based quantum biosensing experiments. In: Proceedings of the 9th military information and communication symposium of South Africa (MICSSA 2023), CSIR. CSIR, pp 29–36. [Online]. Available: https://researchspace.csir.co.za/dspace/handle/10204/13451
136. Ugwuoke LC, Krüger TP, Tame MS (2024) Quantum plasmonics model of refractive index sensing using photon correlations. arXiv:2403.08588
137. Brolo A, Scott J, Gray B, Kavanagh K, Gordon R, Gulzar N, Hohertz D, Romanuik S, Grist S, Nirwan R (2010) A new method for therapeutic antibody screening. SPIE newsroom 10(2.1201006):002995
138. Du B, Yang Y, Zhang Y, Jia P, Ebendorff-Heidepriem H, Ruan Y, Yang D (2019) Enhancement of extraordinary optical transmission and sensing performance through coupling between metal nanohole and nanoparticle arrays. J Phys D: Appl Phys 52(27):275201
139. Liu Y, Zhang X (2011) Metamaterials: a new frontier of science and technology. Chemical Soc Rev 40(5):2494–2507
140. Jain PK, Huang X, El-Sayed IH, El-Sayed MA (2008) Noble metals on the nanoscale: optical and photothermal properties and some applications in imaging, sensing, biology, and medicine. Accounts Chem Res 41(12):1578–1586
141. Kuznetsov AI, Miroshnichenko AE, Brongersma ML, Kivshar YS, Luk'yanchuk B (2016) Optically resonant dielectric nanostructures. Science 354(6314):aag2472
142. Ko JH, Yoo YJ, Lee Y, Jeong H-H, Song YM (2022) A review of tunable photonics: Optically active materials and applications from visible to terahertz. IScience 25(8)
143. Li Y, van de Groep J, Talin AA, Brongersma ML (2019) Dynamic tuning of gap plasmon resonances using a solid-state electrochromic device. Nano Lett 19(11):7988–7995
144. Erdőssy J, Horváth V, Yarman A, Scheller FW, Gyurcsányi RE (2016) Electrosynthesized molecularly imprinted polymers for protein recognition. TrAC Trends Analytical Chem 79:179–190
145. Shumyantseva V, Bulko T, Baychorov I, Archakov A (2016) Molecularly imprinted polymers (mip) in electroanalysis of proteins. Biochemistry (Moscow) Supplement Series B: Biomedical Chemistry 10:145–151
146. Uzun L, Turner AP (2016) Molecularly-imprinted polymer sensors: Realising their potential. Biosensors Bioelectron 76:131–144

147. Bao Y, Shi C, Wang T, Li X, Ma J (2016) Recent progress in hollow silica: Template synthesis, morphologies and applications. Microporous and Mesoporous Mater 227:121–136
148. Ali GK, Omer KM (2022) Molecular imprinted polymer combined with aptamer (mip-aptamer) as a hybrid dual recognition element for bio (chemical) sensing applications. review. Talanta 236:122878
149. Culver HR, Wechsler ME, Peppas NA (2018) Label-free detection of tear biomarkers using hydrogel-coated gold nanoshells in a localized surface plasmon resonance-based biosensor. ACS nano 12(9):9342–9354
150. Svedendahl M, Chen S, Dmitriev A, Kall M (2009) Refractometric sensing using propagating versus localized surface plasmons: a direct comparison. Nano Lett 9(12):4428–4433
151. Yu F, Ahl S, Caminade A-M, Majoral J-P, Knoll W, Erlebacher J (2006) Simultaneous excitation of propagating and localized surface plasmon resonance in nanoporous gold membranes. Analytical Chem 78(20):7346–7350
152. Corporation L (2023) Quantum biosensing technology overview. Accessed: 2024-06-27. [Online]. Available: https://www.youtube.com/watch?v=vOBhQNTp-8U&ab_channel=LamdaGenCorporation
153. Banjara RA, Kumar A, Aneshwari R, Satnami ML, Sinha S (2024) A comparative analysis of chemical vs green synthesis of nanoparticles and their various applications. Environ Nanotechnol, Monitoring Manag, p 100988
154. Osman AI, Zhang Y, Farghali M, Rashwan AK, Eltaweil AS, Abd El-Monaem EM, Mohamed IM, Badr MM, Ihara I, Rooney DW et al (2024) Synthesis of green nanoparticles for energy, biomedical, environmental, agricultural, and food applications: A review. Environmental Chemistry Letters 22(2):841–887
155. Rathod S, Preetam S, Pandey C, Bera SP (2024) Exploring synthesis and applications of green nanoparticles and the role of nanotechnology in wastewater treatment. Biotechnol Reports, pp e00830
156. Arshad F, Naikoo GA, Hassan IU, Chava SR, El-Tanani M, Aljabali AA, Tambuwala MM (2024) Bioinspired and green synthesis of silver nanoparticles for medical applications: a green perspective. Appl Biochem Biotechnol 196(6):3636–3669
157. Shiraz M, Imtiaz H, Azam A, Hayat S (2024) Phytogenic nanoparticles: synthesis, characterization, and their roles in physiology and biochemistry of plants. Biometals 37(1):23–70
158. Lawson ZR (2024) Development of fabrication and synthetic protocols to produce substrate-immobilized plasmonic nanomaterials. Ph.D. dissertation, University of Notre Dame
159. Hang Y, Wang A, Wu N (2024) Plasmonic silver and gold nanoparticles: shape-and structure-modulated plasmonic functionality for point-of-caring sensing, bio-imaging and medical therapy. Chem Soc Rev
160. Kant K, Beeram R, Cabaleiro LG, Cao Y, Quesada-González D, Guo H, Gomez-Grana S, Joung Y, Kothadiya S, García-Lojo D, et al (2024) Roadmap for plasmonic nanoparticle sensors: Current progress, challenges and future prospects. Nanoscale Horizons
161. Tukova A, Nguyen NTT, Garcia-Bennett A, Rodger A, Wang Y (2024) Plasmonic nanostars: Unique properties that distinguish them from spherical nanoparticles from a biosensing perspective. Adv Optical Mater pp 2401183
162. Canning AJ, Li JQ, Atta S, Wang H-N, Vo-Dinh T (2024) Nanoplasmonics biosensors: At the frontiers of biomedical diagnostics. TrAC Trends Analytical Chem, pp 117973
163. Tran VA, Tran TTV, Doan VD, Vo GN, Tran VH, Jeong H, Vo TTT et al (2024) Advanced nano engineering of surface-enhanced raman scattering technologies for sensing applications. Appl Mater Today 38:102217
164. Yang Q, Wu Y, Chen J, Lu M, Wang X, Zhang Z, Xiong H, Choo J, Chen L (2024) Plasmonic nanomaterial-enhanced fluorescence and raman sensors: Multifunctional platforms and applications. Coordination Chem Rev 507:215768
165. Houari F, Talbi A, Mir A, Akjouj A et al (2024) Surface plasmon resonance sensors: Temperature effects. Optical Mater 155:115865
166. Javaid Z, Iqbal MA, Javeed S, Maidin SS, Morsy K, Shati AA, Choi JR (2024) Reviewing advances in nanophotonic biosensors. Front Chem 12:1449161
167. Monfared YE, Qasymeh M (2024) Graphene/titanium nitride hybrid nano-cuboid plasmonic metamaterial–based biosensor for highly sensitive and tunable infrared detection. Plasmonics, pp 1–9
168. Li K, Lin Y-S (2024) Tunable perfect meta-absorber with high sensitivity for refractive index sensing application. Sens Bio-Sens Res 45:100676
169. Verma S, Pathak AK, Rahman BA (2024) Review of biosensors based on plasmonic-enhanced processes in the metallic and metamaterial-supported nanostructures. Micromachines 15(4):502
170. Ma H, Zhang W, Sun T, Song Q, Yi Z, Wu P, Cheng S, Tang C, Zeng Q, Hao Z (2024) High sensitivity and high figure of merit graphene mid-infrared multi-band tunable metamaterial perfect absorber. Surfaces and Interfaces, pp 105137
171. Okamoto K, Tanaka D, Matsuyama T, Wada K, Arima Y, Tamada K (2024) Design and optimization of silver nanostructured arrays in plasmonic metamaterials for sensitive imaging applications. In: Photonics, vol. 11, no. 4. MDPI, pp 292
172. Mollarasouli F, Bahrani S, Amrollahimiyandeh Y, Paimard G (2024) Nanomaterials-based immunosensors for avian influenza virus detection. Talanta pp 126591